Journal of Controlled Release 295 (2019) 223–236

Contents lists available at ScienceDirect

Journal of Controlled Release

journal homepage: www.elsevier.com/locate/jconrel

Heterotelechelic polymer prodrug nanoparticles: Adaptability to different drug combinations and influence of the dual functionalization on the cytotoxicity

Daniele Vinciguerra[a], Merel Jacobs[a], Stéphanie Denis[a], Julie Mougin[a], Yohann Guillaneuf[b], Gianpiero Lazzari[a], Chen Zhu[a], Simona Mura[a], Patrick Couvreur[a], Julien Nicolas[a,*]

[a] Institut Galien Paris-Sud, UMR CNRS 8612, Univ Paris-Sud, Faculté de Pharmacie, 5 rue Jean-Baptiste Clément, F-92296 Châtenay-Malabry cedex, France
[b] Aix Marseille Univ, CNRS, Institut de Chimie Radicalaire UMR 7273, campus Saint Jérôme, Avenue Escadrille Normandie-Niemen, 5 Case 542, 13397 Marseille Cedex 20, France

ARTICLE INFO

Keywords:
Polymer
Nanoparticles
Prodrug
Cancer
Combination therapy
Drug delivery

ABSTRACT

Well-defined, heterotelechelic polymer prodrugs for combination therapy were synthesized by using a combination of the "drug-initiated" nitroxide-mediated polymerization from a gemcitabine-alkoxyamine initiator and the nitroxide exchange reaction using TEMPO-bearing drugs to end-cap the drug-polymer chain-end by a second drug. This methodology was successfully applied to two different clinically relevant combinations, gemcitabine/doxorubicin (Gem/Dox) and gemcitabine/lapatinib (Gem/Lap), showing a certain degree of universality of the synthetic methodology. It also represented the first nanocarrier for the co-delivery of Gem and Lap ever reported. Well-controlled, low molar mass heterotelechelic polymers (M_n = 2100–4090 g.mol^{-1}, $Đ$ = 1.18–1.38) with ~1:1 drug ratios and high overall drug loadings up to 40 wt% were obtained. They were formulated into nanoparticles by nanoprecipitation and exhibited average diameters in the 34–154 nm range, with narrow particle size distributions (PSD = 0.01–0.22) and excellent colloidal stability over time. Their biological evaluation in terms of drug release and cytotoxicity was performed and compared to that of different monofunctional polymer prodrug formulations. We showed that heterobifunctional polymer prodrugs induced cytotoxicity to MCF-7 cells, with IC_{50} values in the 120–300 nM range depending on the combination tested. Interestingly, whereas Gem/Dox combination did not lead to noticeable improvement over monofunctional therapies, co-nanoprecipitation of Gem/Lap prodrugs led to synergistic effect.

1. Introduction

Combination therapy refers to the simultaneous administration of two or more pharmaceutical agents and has shown clear therapeutic benefits to treat different diseases, such as malaria [1,2], HIV [3,4] and cancer [5,6]. Combination therapy offers important advantages compared to monotherapy such as the possibility to modulate different signaling pathways by using drugs with different/complementary mechanisms of actions, which may lead to synergistic effect, and the possibility to overcome resistance mechanisms. For these reasons, combination therapy is commonly associated with improved therapeutic indexes and better long-term prognosis, thanks to enhanced efficacy and/or reduction of the dose of each drug, resulting in less severe side effects and toxicity, which is of prime importance for instance in cancer therapy [7,8].

The main limitation of this approach, however, is that biodistributions and pharmacokinetics can greatly vary from one drug to another, for instance because each drug may have different physico-chemical properties, hydrolytic stabilities, metabolizations, etc. Therefore, precisely controlling the drug ratio until delivery to the right tissues and cells is challenging. To overcome this problem, drugs can be formulated into the same nanocarrier, such as liposomes or polymer nanoparticles, which is expected to maintain the initial drug ratio until cellular internalization [6–9]. However, the traditional encapsulation of drugs into nanocarriers is often associated with important limitations such as the "*burst release*", referring to the quick and sudden release post-administration of a significant amount of drug only surface-adsorbed, which may induce prohibitive toxicity but also strongly vary the drug ratios and the effective drug loading (DL). Also, poor DLs are generally obtained which imposes administration of large amounts of

* Corresponding author.
E-mail address: julien.nicolas@u-psud.fr (J. Nicolas).

https://doi.org/10.1016/j.jconrel.2018.12.047
Received 9 November 2018; Received in revised form 25 December 2018; Accepted 28 December 2018
Available online 03 January 2019

nanocarriers to achieve a therapeutic effect. The "*polymer prodrug*" approach [10,11], whereby the drug is covalently attached to the polymer carrier, aims to solve these limitations. Among the different synthetic pathways to synthesize polymer prodrugs, the recently developed "*drug-initiated*" method [12], relying on the controlled growth of a small polymer chain from a drug-bearing initiator, have indisputable advantages compared to other approaches, such as: (i) a few synthetic steps with high overall yields and reproducibility; (ii) simplified purification procedures; (iii) quantitative functionalization of each polymer chain and (iv) the possibility to tune the DL due to controlled polymerization process and obtain high DLs by targeting short polymer chains.

This technique has been recently applied to different anticancer drugs such as gemcitabine (Gem) [13–16], paclitaxel [17–19] and cladribine [20,21], by reversible-deactivation radical polymerization (RDRP), in particular reversible addition-fragmentation chain transfer (RAFT) polymerization [22] and nitroxide-mediated polymerization (NMP) [23]. In all cases, high drug loading polymer prodrug nanoparticles (up to ~40 wt%) were formulated by nanoprecipitation without any additional surfactant and showed high colloidal stability, significant in vitro cytotoxicity against cancer cells and in vivo efficacy on tumor-bearing mice. Also, different polymers were grown from drugs including polyisoprene [13,17,20], chosen for its biocompatibility and structural similarity with natural terpenoids [24–28], oligo (ethylene glycol) methacrylate [17,21] for its biocompatibility and long-circulating features, and degradable copolymers made by radical ring-opening polymerization [16].

Recently, we proposed a facile synthetic strategy to prepare heterotelechelic polymer prodrugs, embedding two different molecules of interest at both chain-ends and further self-assemble into nanoparticles [29]. The construction methodology relied on the "*drug-initiated*" synthesis of α-functional polymer prodrugs by NMP and subsequent nitroxide exchange reaction [30] to replace the terminal nitroxide by a functional nitroxide bearing the second molecule of interest (Fig. 1a). As proof of concept, we synthesized heterotelechelic polymer prodrugs based on polyisoprene, with either one drug (Gem) and one fluorescent probe (rhodamine) for drug delivery and imaging, either two different drugs (aminoglutethimide and doxorubicin) for combination therapy. The latter heterotelechelic polymer prodrug was formulated into nanoparticles that exhibited lower IC_{50} values than monofunctional counterparts or nanoparticles obtained from the co-nanoprecipitation of the two monofunctional prodrugs [29], in agreement with literature data [31,32]. Although this synthetic methodology appeared to exhibit important benefits, its robustness and versatility, and therefore its future potential in the field of drug delivery, mainly depend on whether it is applicable to other relevant drug combinations.

Herein, because heterotelechelic polymers represent original constructions that could be of great importance in the biomedical field [33], we demonstrate the broad applicability and a certain degree of universality of the "*drug-initiated*" method followed by the nitroxide exchange reaction, by applying it to two different drug combinations of high clinical interest (Fig. 1b): gemcitabine/doxorubicin (Gem/Dox) and gemcitabine/lapatinib (Gem/Lap). Gem is used for the treatment of many solid tumors, such as breast, lung, ovarian and pancreatic cancer [34]. Designing Gem-based prodrugs is particularly relevant because of the very short plasma half-life (8–17 min) of Gem due to rapid metabolization by deaminases [35], induction of severe side effects and appearance of resistance mechanism associated with nucleoside transmembrane transporter [36]. Dox is another extensively used anticancer drug with high efficacy against a wide array of solid tumors such as lung, breast, ovary and thyroid cancers [37]. As for Lap, it is a dual tyrosine kinase inhibitor, able to bind and inhibit epidermal growth factor receptors 1 (EGFR) and 2 (HER2) [38], overexpressed in a variety of cancer type. Nonetheless, it has very poor water solubility, which can be greatly enhanced by formulation into nanocarriers [39–41].

Combination of free Gem and Dox has shown enhanced anticancer efficacy compared to individual monotherapies [42–47], although severe toxicity has been observed in some cases [48–50]. Therefore, polymer-based nanocarriers based on this combination have been reported. For instance, poly(*N*-(2-hydroxypropyl)methacrylamide) (PHPMA) bearing both drugs grafted on the side-chain showed promising in vitro cytotoxicity and in vivo efficacy, although the drug loading was rather modest (~6 wt% for each drug) [51]. On the other hand, poly(ethylene glycol)-*block*-poly(lactic acid) (PEG-*b*-PLA) diblock copolymers were used to either prepare mixed polymer prodrugs nanoparticles with each drug molecule linked to one PLA chain-end (maximum drug loading was ~7 wt%) [52], or PEG-*b*-PLA polymersomes encapsulating both drugs [53]. As for the second combination, we investigated Lap that has recently been approved by the FDA in combination with capecitabin against advanced breast cancer [54–56]. It is capable of reverting some resistance mechanisms and enhancing other drugs' efficacy when co-administered with them [57,58]. The safety of its combination with Gem has been demonstrated in phase I clinical trials [59–62] and more advanced clinical studies demonstrated good response [63] or even complete tumor remission [64]. Still, some concerns about toxicity have been raised [65,66]. To the best of our knowledge, this drug combination has never been delivered using nanocarriers, which could be a way to solve these toxicity issues.

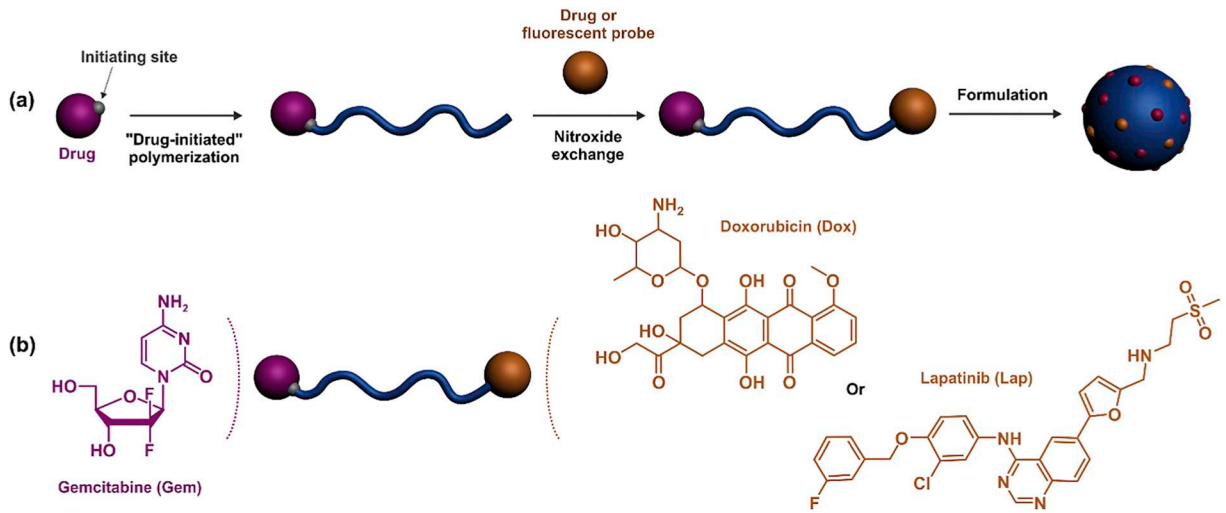

Fig. 1. (a) Synthesis of heterobifunctional polymer prodrugs by "*drug-initiated*" synthesis of polymer prodrugs followed by the nitroxide exchange reaction using a functional nitroxide. (b) Heterotelechelic polymer prodrug bearing either Gem/Dox or Gem/Lap combination.

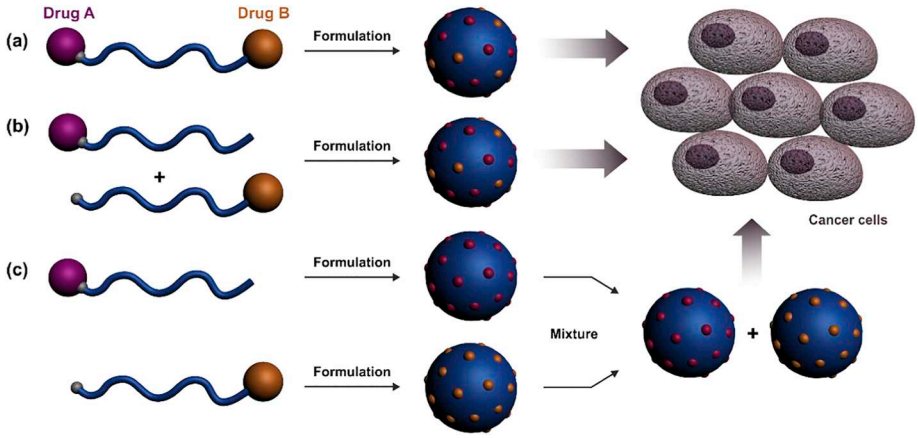

Fig. 2. Formulation strategies to obtain polymer prodrug nanoparticles for combination therapy from: (a) well-defined heterotelechelic polymer prodrugs bearing two different drugs on the same polymer backbone, further nanoprecipitated into nanoparticles; (b) two different monofunctional polymer prodrugs, further *co*-nanoprecipitated into mixed nanoparticles and (c) a physical mixture of two different monofunctional polymer prodrug nanoparticles.

Importantly, it is also admitted that in the case of a multidrug approach, the way each drug is incorporated into a nanocarrier is crucial for the drug release, the activity and the overall benefit of the combination [20,31,51,67,68]. Therefore, different drug-polymer linkers were tested and a comprehensive investigation of the different ways to deliver these combinations was investigated. In particular, we developed and compared: (i) heterotelechelic polymer prodrug nanoparticles (i.e., bearing both drugs on the same polymer backbone); (ii) polymer prodrug nanoparticles obtained by the *co*-nanoprecitation of the two monofunctional polymer prodrugs (i.e., each nanoparticle is carrying both types of polymer prodrugs) and (iii) the physical mixture of the two monofunctional polymer prodrug nanoparticles (i.e., each nanoparticle is carrying one type of polymer prodrug) (Fig. 2).

2. Materials and methods

2.1. Materials

Gemcitabine (> 98%), lapatinib (Lap, 99%) and doxorubicin·HCl (Dox, 99%) were purchased from Carbosynth Limited (UK). Benzotriazol-1-yloxytripyrrolidinophosphonium hexafluorophosphate (PyBOP), *N,N*-diisopropylethylamine (DIPEA), isoprene, 4-(dimethylamino)pyridine (DMAP), succinic anhydride, diglycolic anhydride, triethyl amine, 4-hydroxy-TEMPO, 1-[bis(dimethylamino)methylene]-1H-1,2,3-triazolo[4,5-*b*]pyridinium 3-oxid hexafluorophosphate (HATU), human serum (H4522) were purchased from Sigma-Aldrich (France) and used as received. AMA-SG1 [69] and Gem-AMA-SG1 [13] alkoxyamines, as well as succinic-TEMPO and TEMPO-Dox [29] were prepared as reported previously. All other reactants were purchased from Sigma-Aldrich at the highest available purity and used as received. Deuterated chloroform ($CDCl_3$) was obtained from Eurisotop. All other solvents were purchased from Carlo-Erba at the highest grade. Eagle's Minimum Essential Medium (EMEM) and fetal bovine serum (FBS) were purchased from Dulbecco (Invitrogen, France). Penicillin and streptomycin were obtained from Lonza (Verviers, Belgium). *N*-tert-butyl-*N*-(1-diethylphosphono-2,2-dimethylpropyl) nitroxide (SG1, 85%) was kindly supplied by Arkema.

2.2. Analytical methods

2.2.1. Nuclear magnetic resonance spectroscopy (NMR)

NMR spectroscopy was performed in 5 mm diameter tubes in $CDCl_3$ at 25 °C. ^1H and ^{13}C NMR spectroscopy was performed on a Bruker Avance 300 spectrometer at 300 MHz (^1H) and 75 MHz (^{13}C), respectively. The chemical shift scale was calibrated based on the internal solvent signals. To characterize nitroxide derivatives, pentafluorophenylhydrazine was added in situ and allowed to react before the analysis [70,71].

2.2.2. Mass spectrometry

Mass spectra were recorded with a Bruker Esquire-LC instrument. High-resolution mass spectra (ESI) were recorded on an ESI/TOF (LCT, Waters) LC-spectrometer.

2.2.3. Size exclusion chromatography (SEC)

SEC was performed at 30 °C with two columns from Polymer Laboratories (PL-gel MIXED-D; 300 × 7.5 mm; bead diameter 5 mm; linear part 400 to 4×10^5 g.mol^{-1}), a differential refractive index detector (Spectra System RI-150 from Thermo Electron Corp.) and a scanning fluorescence detector (Waters 474). The eluent was chloroform at a flow rate of 1 mL.min^{-1} (Waters 515 pump) and toluene was used as a flow-rate marker. The calibration curve was based on polystyrene (PS) standards (peak molar masses, M_p = 162–523,000 g.mol^{-1}) from Polymer Laboratories. A polyisoprene (PI) calibration curve was constructed by converting the PS standard peak molecular weights (M_{PS}) to PI molecular weights (M_{PI}) using Mark-Houwink-Sakurada (MHS) constants determined for both polymers in CCl_4 at 25 °C. For PI, the MHS constants used were $K_{PI} = 2.44 \times 10^4$ and $\alpha_{PI} = 0.712$. For PS, $K_{PS} = 7.1 \times 10^4$ and $\alpha_{PS} = 0.54$ ($M_w < 16{,}700$ g.mol^{-1}) or $K_{PS} = 1.44 \times 10^4$ and $\alpha_{PS} = 0.713$ ($M_w > 16{,}700$ g.mol^{-1}) [13]. This technique allowed the number-average molar mass (M_n), the weight-average molar mass (M_w) and the dispersity (M_w/M_n, $Đ$) to be determined.

2.2.4. Dynamic light scattering (DLS) and zeta potential

Intensity-averaged nanoparticle diameters (*Dz*) and zeta potentials (ζ) were measured by dynamic light scattering (DLS) with a Nano ZS from Malvern (173° scattering angle) at a temperature of 25 °C. The surface charge of the nanoparticles was investigated by ζ-potential (mV) measurement at 25 °C after dilution with 1 mM NaCl, using the Smoluchowski equation.

2.2.5. Transmission electron microscopy (TEM)

The morphology of the nanoparticles was observed by TEM using a JEOL JEM-1400 operating at 80 kV. Images were acquired using an Orius camera (Gatan Inc., USA). 5 µL of diluted nanoparticle suspensions (0.1%, *v*/v) were deposited for 30 s on glow-discharged copper grids covered with formvar-carbon film. The excess solution was blotted off using a filter paper. Samples were then immersed for 5 min in a drop of uranyl acetate solution (2 wt%) for negative staining.

2.2.6. Electronic spin resonance (ESR)

ESR was used for the determination of the living fraction (LF) of Gem-PI-Lap and was performed on a Bruker EMX 300 spectrometer. Polyisoprene PI macroalkoxyamine solution ($[PI]_0 = 1.0 \times 10^{-4}$ M) in tert-butylbenzene (0.6 mL) was prepared. The residual amount of nitroxide was first determined by ESR using TEMPO solutions as external

standards. The solution was then heated up at 413 K for 2 h (TEMPO-based macroalkoxyamine) in open air since dioxygen was used as radical scavenger. The solution was then analyzed by ESR and the concentration of the released nitroxide determined using TEMPO solutions as external standards. The LF of the polymer was then obtained by the difference between the nitroxide concentration after and before thermolysis.

2.3. Synthesis

2.3.1. Synthesis of Gem-PI-SG1

Gem-PI-SG1 was synthesized following a procedure previously published by our group [13] and adapted as follows. Isoprene (4.1 mL, 40.8 mmol) and dioxane (4.1 mL) were added to Gem-AMA-SG1 (250 mg, 0.408 mmol) previously placed in a 15 mL-capacity pressure tube (Ace Glass 8648–164) fitted with plunger valve and a thermowell, which then underwent three freeze-pump-thaw cycles and was eventually backfilled with argon. The tube was then placed in a preheated oil bath at 115 °C for 16 h (**G1** and **G4**) and then placed under cold water to stop the polymerization. The volatiles were removed under reduced pressure and the residue was precipitated in cold methanol to give Gem-PI-SG1 as a colorless viscous oil. Other polymerizations were performed for 16 h with $[isoprene]_0/[Gem\text{-}AMA\text{-}SG1]_0$ = 200/1 (**G2**), $[isoprene]_0/[Gem\text{-}AMA\text{-}SG1]_0$ = 300/1 (**G3**) or $[isoprene]_0/[Gem\text{-}AMA\text{-}SG1]_0$ = 550/1 (**G5**). All purified polymers were characterized by SEC and ^{1}H NMR. Conversion was determined by gravimetry: **G1** = 34%, **G2** = 29%, **G3** = 26%, **G4** = 26%, **G5** = 14%.

2.3.2. Synthesis of PI-SG1

Isoprene (6.5 mL, 65.3 mmol) and dioxane (6.5 mL) were added to AMA-SG1 (120 mg, 0.327 mmol) previously placed in a 15 mL-capacity pressure tube (Ace Glass 8648–164) fitted with a plunger valve and a thermowell, which then underwent three freeze-pump-thaw cycles and was eventually backfilled with argon. The tube then was placed in a preheated oil bath at 115 °C for 16 h (**P1**) and then placed under cold water to stop the polymerization. The volatiles were removed under reduced pressure and the residue was precipitated in cold methanol to give PI-SG1 as a colorless viscous oil. The purified polymer was characterized by SEC and ^{1}H NMR. Conversion was determined by gravimetry: **P1** = 24%.

2.3.3. Synthesis of Gem-PI-Dox (G1D-G3D)

In a 7-mL vial were dissolved Gem-PI-SG1 (300 mg, 1 eq) and TEMPO-Dox (0.9 eq) in dry pyridine (1 mL). The solution was degassed under argon for 20 min before placing the vial in a preheated oil bath at 110 °C and stirring for 16 h. Gem-PI-Dox was then precipitated two times in cold methanol and dried under reduced pressure. The post-functionalization yield was calculated by ^{1}H NMR using the chemical shifts of aromatic protons of Dox (δ = 8.15, 7.79 and 7.37 ppm) and the chemical shifts of aromatic and anomeric protons of Gem (δ = 8.26, 7.48 and 6.26 ppm). The post-functionalization was also verified by UV spectrophotometry at 480 nm (Perkin-Elmer UV/vis spectrophotometer, Germany) and SEC equipped with a fluorescent detector (λ_{ex} = 480 nm, λ_{em} = 570 nm).

2.3.4. Synthesis of TEMPO-Lap

To a solution of succinic-TEMPO (0.47 g, 1.72 mmol) and HATU (0.79 g, 2.07 mmol) in dry DMF (5 mL) was added DIPEA (0.9 mL, 5.20 mmol) by syringe under argon atmosphere. The resulting mixture was stirred for 30 min before addition of a solution of lapatinib (1.0 g, 1.72 mmol) in dry DMF (2 mL). The reaction was further stirred at room temperature for 5 h. Water was added and then extracted three times with EtOAc. The combined organic layers were washed with brine, dried over $MgSO_4$ and concentrated under reduced pression. After purification by flash chromatography (SiO_2, DCM:MeOH, 98:2, v:v), 1.1 g of TEMPO-Lap were obtained, as a yellow solid. Yield: 78%. ^{1}H NMR (300 MHz, $CDCl_3$): δ 8.66 (s, 1H), 8.43 (s, 1H), 7.95 (d, 1H), 7.86 (d, 2H), 7.68 (m, 1H), 7.36 (m, 1H), 7.22 (m, 2H), 7.00 (t, 2H), 6.77 (d, 1H), 6.51 (d, 1H), 5.16 (s, 2H), 4.99 – 4.87 (m, 1H), 3.59 – 3.48 (m, 2H), 3.41 (t, 2H), 3.18 (m, 2H), 2.91 (m, 5H), 2.71 (t, 2H), 1.84 (m, 2H), 1.69 – 1.52 (m, 2H), 1.17 (m, 12H). MS (ESI+): m/z = 836.4 $(M)^+$. Calc. for $C_{42}H_{46}ClFN_5O_8S$: 835.4.

2.3.5. Synthesis of Gem-PI-Lap (G1L-G3L)

Briefly, in a 7-mL vial were dissolved Gem-PI-SG1 (300 mg, 1 eq) and TEMPO-Lap (0.9 eq) in dry pyridine (1 mL). The solution was degassed under argon for 20 min before placing the vial in a preheated oil bath at 110 °C and stirring for 16 h. Gem-PI-Lap was then precipitated two times in cold methanol and dried under reduced pressure. All purified polymers were characterized by SEC. The post-functionalization yield was calculated by ESR and ^{1}H NMR using the chemical shifts of aromatic protons of Lap (δ = 8.66, 8.43, 7.95, 7.86, 7.68, 7.36, 7.00, 6.77 and 6.51 ppm) and the chemical shifts of aromatic and anomeric proton of Gem (δ = 8.26, 7.48 and 6.26 ppm).

2.3.6. Synthesis of PI-Dox (D1)

PI-Dox was prepared as reported previously [29]. Briefly, in a 7-mL vial were dissolved PI-SG1 (300 mg, 1 eq) and TEMPO-Dox (0.9 eq) in dry pyridine (1 mL). The solution was degassed under argon for 20 min before placing the vial in a preheated oil bath at 110 °C and stirring for 16 h. PI-Dox was then precipitated two times in cold methanol and dried under reduced pressure. The purified polymer was characterized by SEC. The effectiveness of functionalization was proved qualitatively by ^{1}H NMR and the post-functionalization yield was measured by UV spectrophotometry at 480 nm (Perkin-Elmer UV/vis spectrophotometer, Germany) and SEC equipped with a fluorescent detector (λ_{ex} = 480 nm, λ_{em} = 570 nm).

2.3.7. Synthesis of PI-Lap (L1)

Briefly, in a 7-mL vial were dissolved PI-SG1 (300 mg, 1 eq) and TEMPO-Lap (0.9 eq) in dry pyridine (1 mL). The solution was degassed under argon for 20 min before placing the vial in a preheated oil bath at 110 °C and stirring for 16 h. PI-Lap was then precipitated two times in cold methanol and dried under reduced pressure. The purified polymer was characterized by SEC. The effectiveness of functionalization was proved qualitatively by ^{1}H NMR and the post-functionalization yield was measured by ESR.

2.3.8. Synthesis of digly-TEMPO (2-(2-((1-oxyl-2,2,6,6-tetramethylpiperidin-4-yl)oxy)-2-oxoethoxy)acetic acid)

A solution of 4-hydroxy-TEMPO (1.0 g, 5.80 mmol), diglycolic anhydride (1.68 g, 14.5 mmol) and triethylamine (4.04 mL, 29.0 mmol) in DCM (20 mL) was stirred 4 h at room temperature under argon atmosphere. The mixture was then washed with 1 M HCl and brine before being dried over $MgSO_4$. The residue was concentrated under reduced pressure to give 1.30 g of Digly-AMA-SG1 as a sticky solid. Yield = 77%. ^{1}H NMR (300 MHz, $CDCl_3$): δ 5.20 (m, 1H), 4.18 (s, 2H), 4.11 (s, 2H), 2.18 (d, 2H), 1.99 (t, 2H), 1.41 (s, 6H), 1.37 (s, 6H). MS (ESI-): m/z = 288.2 $(M)^+$. Calc. for $C_{13}H_{22}NO_6$: 288.1.

2.3.9. Synthesis of TEMPO-digly-Dox

To a solution of digly-TEMPO (0.45 g, 1.56 mmol) and HATU (0.71 g, 1.87 mmol) in dry DMF (5 mL) was added DIPEA (0.8 mL, 4.68 mmol) by syringe under argon atmosphere. The resulting mixture was further stirred for 30 min before addition of a solution of doxorubicin·HCl (0.91 g, 1.56 mmol) in dry DMF (2 mL). The reaction was stirred at room temperature for 4 h. Water was added (50 mL) and then extracted three times with EtOAc. The combined organic layers were washed with brine, dried over $MgSO_4$ and concentrated under reduced pression. After purification by flash chromatography (SiO_2, DCM:MeOH, 98:2, v:v), 0.37 g of TEMPO-digly-Dox were obtained as a red-orange solid. Yield: 31%. ^{1}H NMR (300 MHz, $CDCl_3$): δ 8.04 (d,

1H), 7.80 (t, 1H), 7.41 (d, 1H), 6.11 (b, 1H), 5.54 (s, 1H), 5.31 (s, 1H), 5.05 – 4.98 (m, 1H), 4.78 (s, 2H), 4.72 – 4.62 (m, 1H), 4.22 (s, 2H), 4.14 (s, 2H), 4.09 (s, 3H), 3.70 (s, 1H), 2.39 (m, 2H), 2.18 (m, 2H), 2.03-1.75 (m, 6H), 1.51 (s, 3H), 1.48 (s, 12H). MS (ESI+): m/z = 836.6 $(M + Na)^+$. Calc. for $C_{40}H_{49}N_2O_{16}$: 813.31.

2.3.10. Synthesis of TEMPO-digly-Lap

To a solution of digly-TEMPO (0.22 g, 0.76 mmol) and HATU (0.35 g, 0.91 mmol) in dry DMF (5 mL) was added DIPEA (0.4 mL, 2.28 mmol) by syringe under argon atmosphere. The resulting mixture was stirred for 30 min before addition of a solution of Lap (0.44 g, 0.76 mmol) in dry DMF (2 mL). The reaction was further stirred at room temperature for 4 h. Water was added (50 mL) and then extracted three times with EtOAc. The combined organic layers were washed with brine, dried over $MgSO_4$ and concentrated under reduced pression. After purification by flash chromatography (SiO_2, DCM:MeOH, 96:4, v:v), 0.32 g of TEMPO-digly-Lap were obtained, as a yellow solid. Yield: 50%. ^{1}H NMR (300 MHz, $CDCl_3$): δ 8.69 (s, 1H), 8.43 (s, 1H), 7.91 (q, 3H), 7.71 (d, 1H), 7.37 (m, 1H), 7.24 (m, 2H), 7.01 (m, 2H), 6.76 (s, 1H), 6.52 (s, 1H), 5.16 (s, 2H), 4.99 – 4.87 (m, 1H), 4.75 (s, 2H), 4.51 (s, 2H), 3.73 – 3.62 (m, 2H), 3.50 – 3.35 (m, 2H), 2.99 (m, 5H), 1.90 (m, 2H), 1.71 (m, 2H), 1.23 (m, 12H). MS (ESI+): m/z = 851.3 $(M)^+$. Calc. for $C_{42}H_{46}ClFN_5O_9S$: 850.3.

2.3.11. Synthesis of Gem-PI-digly-Dox (G4dD, G5dD)

In a 7-mL vial were dissolved Gem-PI-SG1 (300 mg, 1 eq) and TEMPO-digly-Dox (1 eq) in dry pyridine (1 mL). The solution was degassed under argon for 20 min before placing the vial in a preheated oil bath at 110 °C and stirring for 16 h. Gem-PI-digly-Dox was then precipitated two times in cold methanol and dried under reduced pressure. The post-functionalization yield was calculated by ^{1}H NMR using the chemical shifts of aromatic protons of Dox (δ = 8.15, 7.79 and 7.37 ppm) and the chemical shifts of aromatic and anomeric proton of Gem (δ = 8.26, 7.48 and 6.26 ppm). The post-functionalization was also verified by SEC equipped with a fluorescent detector (λ_{ex} = 480 nm, λ_{em} = 570 nm).

2.3.12. Synthesis of Gem-PI-digly-Lap (G1dL, G3dL)

In a 7-mL vial were dissolved Gem-PI-SG1 (300 mg, 1 eq) and TEMPO-digly-Lap (1 eq) in dry pyridine (1 mL). The solution was degassed under argon for 20 min before placing the vial in a preheated oil bath at 110 °C and stirring for 16 h. Gem-PI-digly-Lap was then precipitated two times in cold methanol and dried under reduced pressure. All purified polymers were characterized by SEC. The post-functionalization yield was calculated by ^{1}H NMR using the chemical shifts of aromatic protons of Lap (δ = 8.66, 8.43, 7.95, 7.86, 7.68, 7.36, 7.00, 6.77 and 6.51 ppm) and the chemical shifts of aromatic and anomeric proton of Gem (δ = 8.26, 7.48 and 6.26 ppm).

2.4. Nanoparticle preparation

All nanoparticles were prepared by the nanoprecipitation technique [72]. For **P1**, **G2**, **G4dD**, **G5dD**, **G1dL** or **G3dL**, 2.5 mg of the corresponding polymer prodrug were dissolved in 0.5 mL of THF and quickly added to 1 mL of MilliQ water. For **L1**, 2 mg of polymer prodrug were dissolved in 5 mL of THF and quickly added to 10 mL of MilliQ water. The resulting nanoparticles (**L1**) where then subjected to a x10 concentration under reduced pressure. For **D1**, **G1D**, **G2D**, **G3D**, **G2coD1**, **G1L**, **G2L**, **G3L** and **G2coL1**, 1 mg of the corresponding polymer prodrug was dissolved in 0.5 mL of THF and quickly added to 1 mL of MilliQ water. For co-nanoprecipitations, the ratio between the different polymer prodrugs was 1:1 (mol:mol). THF was evaporated at ambient temperature using a Rotavapor. Intensity-averaged diameter (D_z) and zeta potential measurements were carried out in triplicate by DLS. The nanoparticle colloidal stability was assessed in water for 30 days. The nanoparticles were kept at 4 °C and allowed to reach room temperature before each measurement.

2.5. Gemcitabine release

Gem release kinetics was determined by using the following protocol. 0.2 mL of each nanoparticle suspension (**G2**, **G2D**, **G2coD1**, **G5dD**, **G2L**, **G2coL1** or **G3dL**) were added to 0.8 mL of human serum supplemented with 200 $\mu g.mL^{-1}$ tetrahydrouridine (THU) [20,73]. The mixture was aliquoted (100 µL), incubated at 37 °C, withdrawn at different time points (1, 2, 4, 8 and 24 h), spiked with 10 µL of 10 µM theophylline (Internal Standard, IS) before addition of 1 mL of a mixture of acetonitrile:methanol (90:10, v:v) and ultracentrifugated (15,000 g, 20 min, 4 °C). The supernatant was then evaporated to dryness under a nitrogen flow at 30 °C and the released drug was quantified by reverse-phase HPLC. The chromatographic system was composed of a Waters 1525 Binary HPLC pump, a Waters 2707 Autosampler, a C18 Uptisphere column (3 µm, 150 × 4.6 mm; Interchim), HPLC column temperature controllers (model 7950 column heater and chiller; Jones Chromatography, Lakewood, CO) and a Waters 2998 programmable photodiode-array detector. The HPLC column was maintained at 30 °C and detection was monitored at 270 nm. The HPLC mobile phase was a mixture of methanol:water with 0.05 M sodium acetate (pH 5.0, eluent A: 5:95, v:v; eluent B: 97:3, v:v). The residues were dissolved in 100 µL of eluent A. Elution was performed at a flow rate of 0.8 $mL.min^{-1}$ isocratically for 8 min with eluent A followed by a linear gradient (1 min) to 75% eluent A and kept isocratically for 6 min at 75% eluent A. A linear gradient (1 min) to 100% eluent B was followed by 10 min of isocratic gradient at 100% eluent B. After a linear gradient (1 min) to 100% eluent A, the system was held for 7 min for equilibration back to initial conditions.

2.6. Cell lines and cell culture

Human breast cancer cell line MCF-7 was obtained from the American Type Culture Collection (ATCC) and maintained as recommended. Briefly, MCF-7 cells were grown in Eagle's Minimum Essential Medium (EMEM), supplemented with 10% heat-inactivated FBS (56 °C, 30 min), penicillin (100 $U.mL^{-1}$) and streptomycin (100 $\mu g.mL^{-1}$), 1% non-essential amino acids (NEAA) and 5 mL glutamine. Cells were maintained in a humid atmosphere at 37 °C with 5% CO_2.

2.7. In vitro anticancer activity

The MTT [3-(4,5-dimethylthiazol-2-yl)-2,5-diphenyl tetrazolium bromide] assay was used to evaluate the cytotoxicity of the different polymer prodrug nanoparticles. Cells (5×10^3 per well) were seeded in 96-well plates. After an overnight incubation, cells were exposed to a series of increasing concentrations of polymer prodrug nanoparticles, control polymers or free drugs for 72 h. Note that for dual functionalized polymer prodrug nanoparticles, the concentration refers to the concentration of each drug. At the end of the exposure time, 20 µL of MTT solution (5 $mg.mL^{-1}$ in PBS) were then added in each well. Plates were incubated for 1 h at 37 °C followed by removal of the medium and addition of 200 µL of DMSO to each well to dissolve the formazan crystals. Absorbance was measured at 570 nm using a plate reader (Metertech Σ 960, Fisher Bioblock, Illkirch, France). The percentage of surviving cells was calculated as the absorbance ratio of treated to untreated cells. The inhibitory concentration 50% (IC_{50}) of the treatments was determined from the dose-response curve. All experiments were repeated at least three times (6 replicates per condition) to determine means and SDs. A Student's *t*-test was used to determine statistical differences.

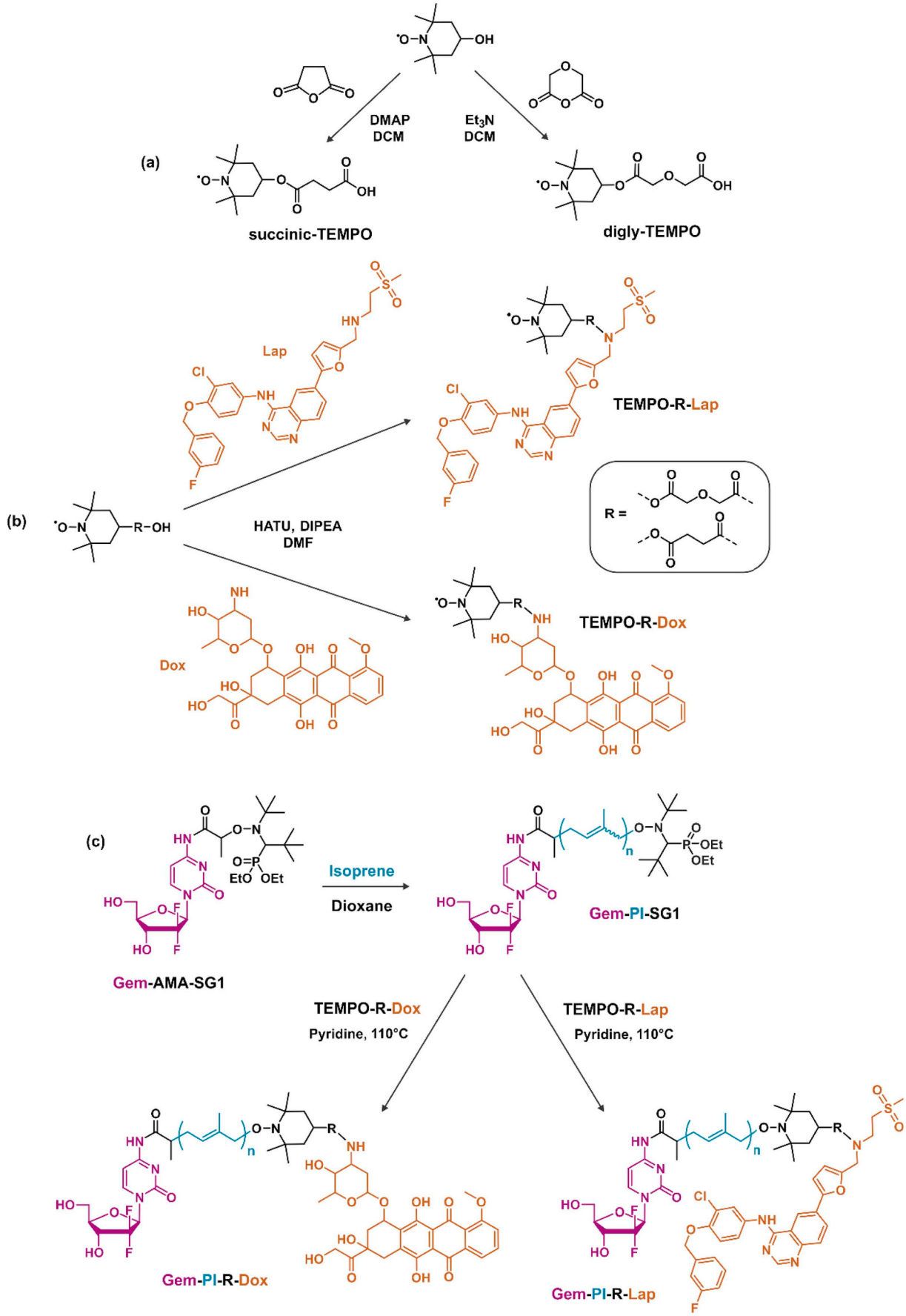

Scheme 1. (a) Synthesis of succinic-TEMPO and digly-TEMPO. (b) Synthesis of TEMPO-R-Dox and TEMPO-R-Lap. (c) Synthesis of heterobifunctional Gem-PI-R-Dox and Gem-PI-R-Lap polymer prodrugs by "*drug-initiated*" nitroxide-mediated polymerization (NMP) of isoprene from Gem-AMA-SG1 followed by nitroxide exchange from TEMPO-R-Dox and TEMPO-R-Lap. PI = polyisoprene, Gem = gemcitabine, Dox = doxorubicin and Lap = lapatinib.

3. Results and discussion

3.1. Design rationale

The synthesis of heterotelechelic Gem/Lap and Gem/Dox polymer prodrugs proceeded according to the polymerization of isoprene from a SG1-containing, Gem-bearing alkoxyamine initiator for NMP, followed by SG1 exchange reaction by a Dox- or Lap-bearing TEMPO nitroxides to yield Gem-PI-Dox and Gem-PI-Lap, respectively (Scheme 1). PI was selected for its biocompatibility and safety, as already demonstrated both in vitro and in vivo [13,17,20,29]. Among the different post-functionalization strategies that can be applied to NMP-derived polymers (i.e., end-capped by a nitroxide) [23], the nitroxide exchange reaction has been selected for its simplicity and feasibility [30]. It consists in a thermally-governed replacement of the nitroxide at the chain-end by a free nitroxide of different nature, driven by the establishment of a less labile polymer-nitroxide (i.e., macroalkoxyamine) bond. The advantages of this methodology lied in: (i) the absence of catalyst, other reactants or by-products except the released nitroxide; (ii) a simple workup; (iii) very high/quantitative yields allowing stoichiometric amounts of free nitroxide to be used and (iv) the use of functional free nitroxides to provide easy access to end-functional materials.

From now on, the different nanoparticles will be abbreviated as follows (with x = 1–5): PI-SG1 (**Px**), Gem-PI (**Gx**), PI-Dox (**Dx**), Gem-PI-Dox (**GxD**), PI-Lap (**Lx**), Gem-PI-Lap (**GxL**), Gem-PI-digly-Dox (**GxdD**) and Gem-PI-digly-Lap (**GxdL**). Polymer prodrug nanoparticles obtained by co-nanoprecipitation of **G2** and **L1** (or **D1**) will be abbreviated as **G2coL1** (or **G2coD1**). Mixture of monofunctional polymer prodrug nanoparticles **G2** and **L1** (or **D1**) will be abbreviated as **G2** + **L1** (or **G2** + **D1**).

3.2. Polymer prodrug synthesis

Gem was first covalently linked to the AMA-SG1 alkoxyamine to give Gem-AMA-SG1. Then, it served as initiator/controlling agent for the NMP of isoprene to yield a small library of α-functionalized Gem-PI (**G1-G3**), obtained by varying the monomer/initiator molar ratio. Well-controlled Gem-bearing polymers were obtained as M_n values (SEC), varying from 1930 to 3840 g.mol^{-1} with low dispersities ($Đ$ = 1.18–1.33). Given the low M_n, it resulted in high drug loadings up to nearly 14 wt% (Scheme 1c and Table 1). Note that the drug-loading could be further increased if needed just by decreasing the PI chain length, which is readily achievable by using RDRP.

Heterotelechelic polymer prodrugs were then obtained by the nitroxide exchange reaction from a functional TEMPO nitroxide bearing the second drug of interest. To this end, succinic-TEMPO was linked, by HATU coupling, to Dox and Lap to give TEMPO-Dox (45% yield) or TEMPO-Lap (78% yield), respectively (Scheme 1b). The nitroxide exchange reaction was then performed in pyridine at 110 °C to post-functionalize **G1-G3** into Gem-PI-Dox (**G1D-G3D**) or Gem-PI-Lap (**G1L-G3L**) as shown in Scheme 1c and Table 1. Considering the LF of Gem-PI-SG1 is ~80 mol% [29], only 0.9 eq of functionalized TEMPO was used to facilitate the purification of the heterobifunctional polymer. The nitroxide exchange reaction was monitored by SEC and ^{1}H NMR. Nearly perfect overlays of the SEC traces (DRI detector) of Gem-PI prodrugs **G1-G3** with those of the resulting heterobifunctional prodrugs **G1D-G3D** and **G1L-G3L** indicated that no or marginal occurrence of side/termination reactions happened during the nitroxide exchange (Figs. 3a and S1). Moreover, by using the intrinsic fluorescence of Dox, SEC traces of **G1D-G3D** using a fluorescence detector exhibited similar molar mass distributions than their DRI traces, thus indicating homogeneous chain-end functionalization by TEMPO-Dox (Figs. 3b and S2).

^{1}H NMR was used to quantify the amount of Dox and Lap present at the polymer chain-end (Figs. 4 and 5). The aromatic peaks of Dox (δ = 8.15, 7.79 and 7.37 ppm) and Lap (δ = 8.66, 8.43, 7.95, 7.86, 7.68, 7.36, 7.00, 6.77 and 6.51 ppm) were compared to the aromatic and anomeric peaks of Gem (δ = 8.26, 7.48 and 6.26 ppm) to calculate the yields of the nitroxide exchange reaction, which were almost quantitative in all cases (100–92 mol%). This indicates a nearly 1:1 (mol:mol) ratio between Gem/Lap and Gem/Dox. The completeness of the reaction was also supported by the total disappearance of the proton signal related to the proton in α position to the phosphorous atom of the SG1 nitroxide (3.2–3.4 ppm).

Electron spin resonance (ESR) has proved to be a suitable technique to study the nitroxide exchange reaction [29]. Therefore, ESR was used to measure the amount of released TEMPO-Lap from Gem-PI-Lap after heating at 413 K for 2 h. The molar fraction of released TEMPO-Lap was found to be ~59–64 mol% from **G1L–G3L**, which gave ~74–80 mol% coupling efficiency after taking into account the living fraction of Gem-PI-SG1 (~80 mol%) [29]. Note that the discrepancy between ^{1}H NMR and ESR in the determination of Lap contents may be assigned to the relative inaccuracy in the determination of M_n values that are required for ESR conversely to ^{1}H NMR that does not rely on any calibration. ESR also confirmed high purity of Gem-PI-Lap as no signal of free nitroxide was found; neither SG1 or TEMPO before heating nor free SG1 after

Table 1
Macromolecular and structural properties of Gem-PI (Gx), Gem-PI-Dox (GxD) and Gem-PI-Lap (GxL) polymer prodrugs (x = 1–3).

Prodrug	$M_{n,SEC}$[a] (g.mol^{-1})	$Đ$[a]	$M_{n,NMR}$ (g.mol^{-1})	$DP_{n,NMR}$[e]	Dox/Gem[f]	Lap/Gem[f]	Total drug loading (wt%)[g]	Lap[h] (mol.%)	Dox[i] (mol.%)
G1	1930	1.33	1830[b]	18	–	–	13.6	–	–
G2	2880	1.20	2450[b]	27	–	–	9.1	–	–
G3	3840	1.18	2940[b]	34	–	–	6.8	–	–
G1D	2210	1.38	3190[c]	30	1.08	–	36.5	–	65
G2D	3210	1.24	3800[c]	40	1.06	–	25.1	–	62
G3D	4090	1.23	4410[c]	48	1.02	–	19.7	–	62
G1L	2100	1.29	2760[d]	24	–	0.96	40.2	64	–
G2L	3060	1.19	4020[d]	42	–	0.92	27.6	60	–
G3L	3890	1.18	4970[d]	56	–	0.93	21.7	59	–

[a] Determined by SEC, calibrated with PS standards and converted into PI by using Mark-Houwink-Sakurada parameters.
[b] Calculated according to $M_{n,NMR} = (DP_{n,NMR} \times MW_{isoprene}) + MW_{Gem\text{-}AMA\text{-}SG1}$.
[c] Calculated according to $M_{n,NMR} = (DP_{n,NMR} \times MW_{isoprene}) + MW_{Gem\text{-}AMA\text{-}SG1} - MW_{SG1} + MW_{TEMPO\text{-}Dox}$.
[d] Calculated according to $M_{n,NMR} = (DP_{n,NMR} \times MW_{isoprene}) + MW_{Gem\text{-}AMA\text{-}SG1} - MW_{SG1} + MW_{TEMPO\text{-}Lap}$.
[e] Calculated from ratio of areas under the peak at 6.1–6.3, 7.3–7.5, 8.0–8.2 ppm (aromatic and anomeric proton of Gem) and 5.0–5.5 ppm (vinylic H in isoprene repeat unit (1,4-addition), corresponding to ~81% of total isoprene units).
[f] Calculated by ^{1}H NMR (see experimental part).
[g] Calculated according to $MW_{Gem}/M_{n,SEC}$ (**G1–G3**), $(MW_{Gem} + MW_{Dox})/M_{n,SEC}$ (**G1D–G3D**) and $(MW_{Gem} + MW_{Lap})/M_{n,SEC}$ (**G1L–G3L**).
[h] Determined by ESR.
[i] Determined by UV spectroscopy.

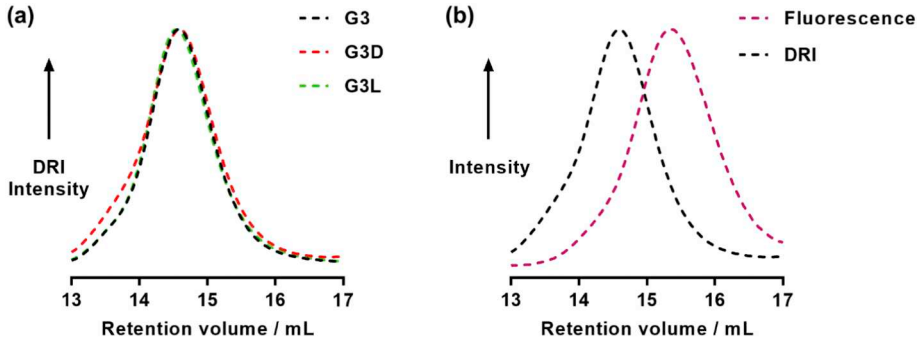

Fig. 3. Size exclusion chromatograms ($CHCl_3$ eluent, 1 mL.min^{-1}) of (a) Gem-PI-SG1 (**G3**, black dashed line), Gem-PI-Dox (**G3D**, red dashed line) and Gem-PI-Lap (**G3L**, green dashed line) and (b) Gem-PI-Dox (**G3D**) fluorescence (purple dashed line) and DRI (black dashed line) after nitroxide exchange (the gap in retention volume between DRI and fluorescence traces comes from the tubing between the two detectors). (For interpretation of the references to colour in this figure legend, the reader is referred to the web version of this article.)

dissociation (Fig. S3). It was however not possible to have a reliable and thus accurate quantification of the exchange conversion by ESR from Gem-PI-Dox, likely because the quinone ring of Dox acted as a radical scavenger. The coupling of TEMPO-Dox was alternatively measured by UV spectroscopy based on a calibration curve using free Dox. The amount of Dox was also found in the 62–65 mol% range, which gave 78–81 mol% coupling efficiency.

The nitroxide exchange reaction was also used to synthesize monofunctional polymer prodrugs used as control polymers: PI-Dox (**D1**) and PI-Lap (**L1**) were obtained from the reaction between PI-SG1 (**P1**) and TEMPO-Dox or TEMPO-Lap, respectively (Table 2). Dispersities of the resulting prodrugs stayed low (1.12–1.22) and their SEC traces compared to that of the polymer precursor did not reveal significant change in the molar mass distributions (Fig. S4a). Also, comparison between DRI and fluorescence traces indicated homogeneous chain-end functionalization by TEMPO-Dox moieties (Fig. S4b). ^{1}H NMR spectroscopy only served to qualitatively prove the presence of Dox and Lap at the polymer chain-end, but not quantitatively to determine the nitroxide exchange reaction yield because of lack of suitable protons in α-position to the polymer (Figs. S5 and S6). Nonetheless, the amount of Lap linked to the polymer was determined by ESR showing 75% coupling yield, whereas UV spectroscopy gave 65% functionalization yield for Dox, which is in line with the other Dox-functionalized polymers. Given the low M_n and the molecular weights of the drugs, drug loadings of 17 and 19 wt% were obtained for **D1** and **L1**, respectively.

To establish the versatility of the synthetic approach and potentially to increase the drug release kinetics (and therefore the cytotoxicity), a diglycolate linker, known to be more labile than a simple ester or amide bond [17,20,21,74], was positioned in between TEMPO and Dox (or Lap). The synthetic route was identical to that used previously except hydroxy-TEMPO was reacted with diglycolic anhydride instead of succinic anhydride to give digly-TEMPO with a 77% yield (Scheme 1a). It was then functionalized with Dox and Lap via HATU coupling to give TEMPO-digly-Dox and TEMPO-digly-Lap, with 31 and 50% yield, respectively (Scheme 1b). Gem-PI-digly-Dox **G4dD** and **G5dD**, only differing for their M_n, were successfully obtained by reacting TEMPO-digly-Dox with Gem-PI-SG1 **G4** and **G5**, respectively (Scheme 1c and Table S1). Gem-PI-digly-Lap **G1dL** and **G3dL** were similarly obtained by reacting TEMPO-digly-Lap on **G1** and **G3**, respectively (Scheme 1c

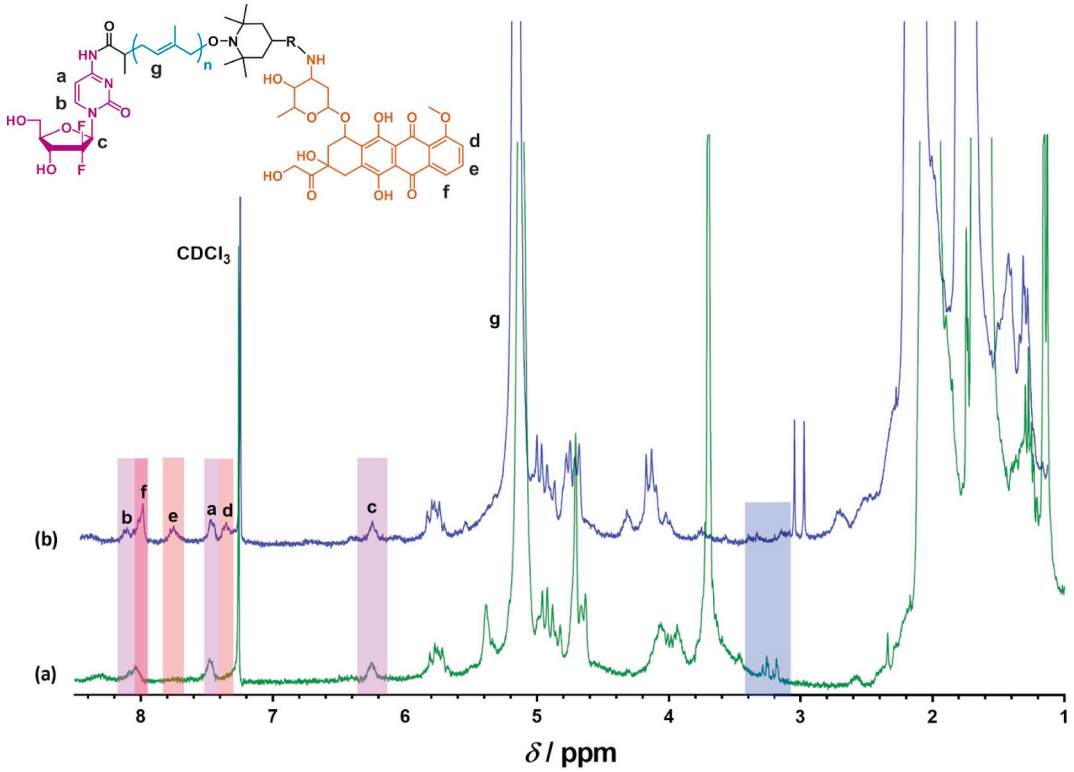

Fig. 4. Representative ^{1}H NMR spectrum in $CDCl_3$ in the 1–8.5 ppm region of (a) Gem-PI-SG1 (**G2**) and (b) Gem-PI-Dox (**G2D**), with R = succinate. After nitroxide exchange with TEMPO-Dox, the proton signals from Dox (orange areas) appeared, those from Gem are retained (purple areas) and those from SG1 (blue area) disappeared. (For interpretation of the references to colour in this figure legend, the reader is referred to the web version of this article.)

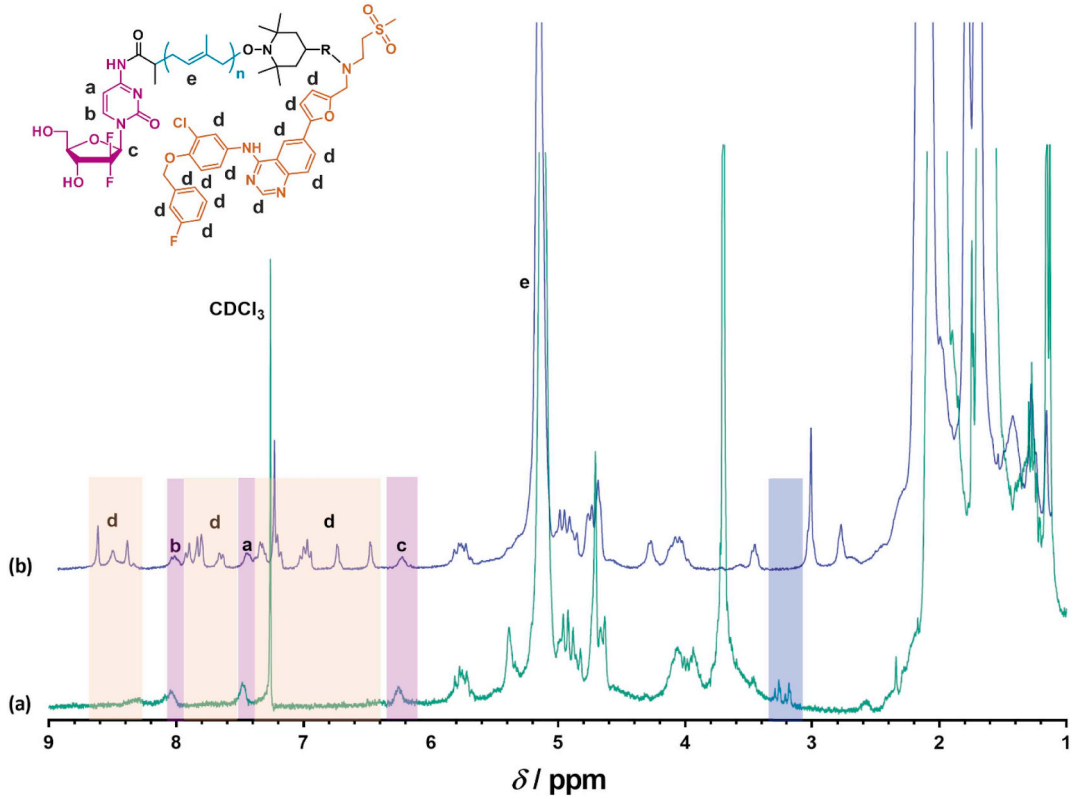

Fig. 5. Representative ^{1}H NMR spectrum in $CDCl_3$ in the 1–9 ppm region of (a) Gem-PI-SG1 (**G2**) and (b) Gem-PI-Lap (**G2L**), with R = succinate. After nitroxide exchange with TEMPO-Lap, the proton signals from Lap (orange areas) appeared, those from Gem are retained (purple areas) and those from SG1 (blue area) disappeared. (For interpretation of the references to colour in this figure legend, the reader is referred to the web version of this article.)

Table 2
Macromolecular characterization of PI-SG1 (**P1**), PI-Dox (**D1**) and PI-Lap (**L1**) polymer prodrugs.

Prodrug	$M_{n,SEC}$[a] (g.mol^{-1})	$Đ$[a]	Drug loading (wt %)[b]	Lap[c] (mol. %)	Dox[d] (mol. %)
P1	2860	1.13	–	–	–
D1	3220	1.22	16.7	–	65
L1	3060	1.12	19.0	75	–

[a] Determined by SEC, calibrated with PS standards and converted into PI by using Mark-Houwink-Sakurada parameters.
[b] Calculated according to $MW_{Dox}/M_{n,SEC}$ (**D1**) and $MW_{Lap}/M_{n,SEC}$ (**L1**).
[c] Determined by ESR.
[d] Determined by UV spectroscopy.

and Table S1). Polymer prodrug characterizations by SEC (Fig. S7) and ^{1}H NMR (Figs. S8 and S9) confirmed the formation of the expected structures.

3.3. Nanoparticle formulation and colloidal properties

Bare (drug-free), monofunctional and heterobifunctional polymer (prodrug) nanoparticles were obtained by nanoprecipitation of the respective polymers in water without any surfactant (Table 3). All types of nanoparticles showed small average diameters and narrow particle size distributions (PSD). Moreover, the surface charges of all nanoparticles were strongly negative, which is usually a premise of an efficient colloidal stability. Bare nanoparticles were 118 nm in diameter, while monofunctional prodrug nanoparticles were much smaller (D_z = 49–68 nm), likely because of an increased amphiphilicity of the polymer after its coupling to the drug. Mixed polymer prodrug nanoparticles **G2coD1** and **G2coL1** had a larger average diameter of 91 and 192 nm, respectively.

Table 3
Characterization of Gem-PI (**Gx**), Gem-PI-Dox (**GxD**), PI-Dox (**Dx**), Gem-PIcoPI-Dox (**G2coD1**), Gem-PI-Lap (**GxL**), PI-Lap (**Lx**) and Gem-PIcoPI-Lap (**G2coL1**) prodrug nanoparticles (x = 1–3).

Prodrug	D_z[a] (nm)	PSD[a]	ζ[a] (mV)	Gem[b] (wt%)	Dox[c] (wt%)	Lap[d] (wt%)	Total drug loading (wt %)
P1	118 ± 2	0.14	−29	–	–	–	–
G2	68 ± 1	0.13	−29	9.1	–	–	9.1
D1	66 ± 2	0.15	−44	–	16.9	–	16.9
L1	49 ± 3	0.12	−36	–	–	19.0	19.0
G1D	34 ± 3	0.22	−32	11.9	24.6	–	36.5
G2D	43 ± 2	0.16	−35	8.2	16.9	–	25.1
G3D	37 ± 1	0.14	−24	6.4	13.3	–	19.7
G2coD1	91 ± 2	0.13	−41	4.3	8.9	–	13.2
G1L	73 ± 1	0.03	−23	12.5	–	27.7	40.2
G2L	154 ± 3	0.01	−27	8.6	–	19.0	27.6
G3L	103 ± 1	0.04	−29	6.8	–	14.9	21.7
G2coL1	192 ± 4	0.17	−47	4.4	–	9.8	14.2

[a] Measured by dynamic light scattering (DLS). Nanoparticle concentration was: 2.5 mg.mL^{-1} for **P1**, **G2**, **G4dD**, **G5dD**, **G1dL**, **G3dL**; 1 mg.mL^{-1} for **D1**, **G1D–G3D**, **G2coD1**, **G1L–G3L** and **G2coL1**, and 2 mg.mL^{-1} for **L1**.
[b] Calculated according to $MW_{Gem}/M_{n,SEC}$.
[c] Calculated according to $MW_{Dox}/M_{n,SEC}$.
[d] Calculated according to $MW_{Lap}/M_{n,SEC}$.

Interestingly, heterotelechelic polymer prodrug nanoparticles **G1D-G3D** exhibited very small diameters around 40 nm, likely because of π-π stacking interactions between Dox molecules, leading to more packed nanoparticles. For the first time, nanoparticles containing the Gem/Lap combination (**G1L-G3L**) were formulated. They presented an average diameter ranging from 73 to 154 nm with no correlation between the polymer molar mass and the nanoparticle size. The nanoparticles were also analyzed by TEM, showing spherical morphologies and size in

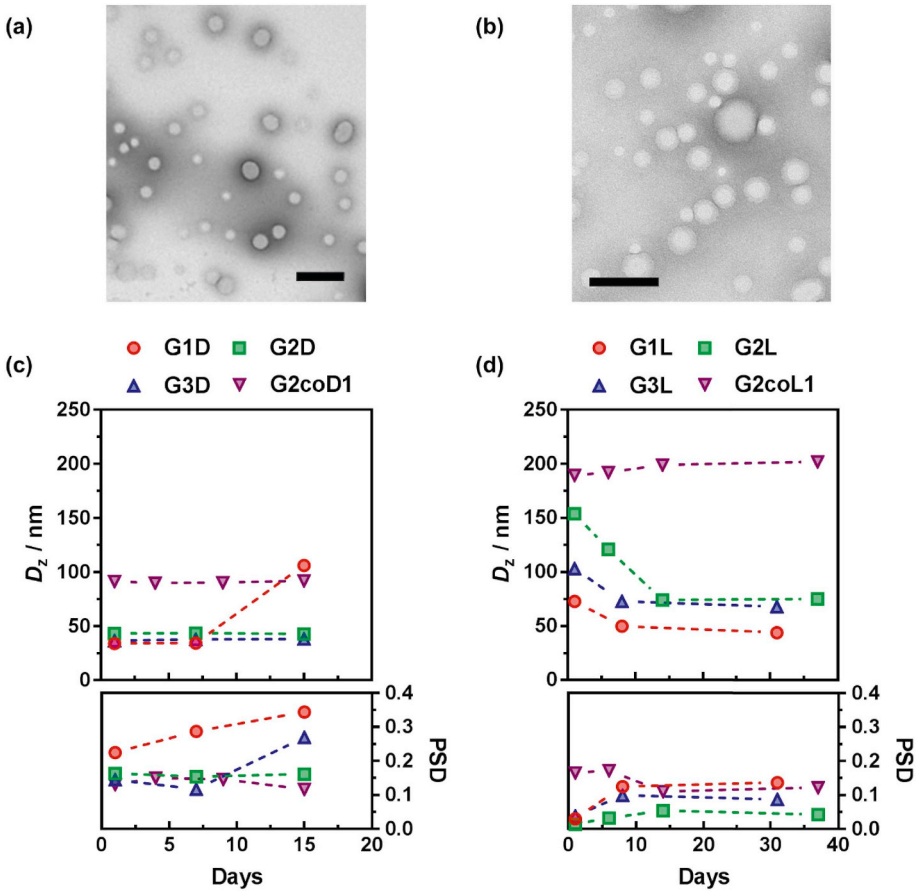

Fig. 6. Representative TEM images of (a) Gem-PI-Dox nanoparticles **G3D** (scale bar = 1 μm) and (b) Gem-PI-Lap nanoparticles **G2L** (scale bar = 0.5 μm). Evolution of the average diameters (D_z) and the particle size distributions (PSD) measured by DLS in water of (c) Gem-PI-Dox nanoparticles (**G1D**, **G2D**, **G3D** and **G2coD1**) and (d) Gem-PI-Lap nanoparticles (**G1L**, **G2L**, **G3L** and **G2coL1**).

agreement to those determined by DLS (Fig. 6a and b).

An important characteristic of heterotelechelic polymers is the ability to yield high drug loading nanoparticles. Here nanoparticles embedding two drugs reached a total DL ranging from ~20 wt% up to ~40 wt%, which is much higher than traditional drug-loaded nanoparticles and most of polymer-prodrug nanoparticles. Also, formulation of heterobifunctional polymer prodrugs is much advantageous in terms of DL than the *co*-nanoprecipitation of monofunctional polymer prodrugs because more polymer is needed in the latter case to reach an equivalent dose of drugs, thus lowering the DL.

The long-term colloidal stability of Gem/Dox and Gem/Lap nanoparticles was monitored in water (Fig. 6c and d, respectively). Gem-PI-Dox (**G2D** and **G3D**) and **G2coD1** nanoparticles were stable over 15 days whereas **G1D** was stable up to 7 days. The less efficient stability of **G1D** could be attributed to the modified hydrophilic-lipophilic balance because of the shorter polymer chain. Gem-PI-Lap (**G1L-G3L**) and **G2coL1** nanoparticles were all stable over more than one month. Interestingly, heterobifunctional polymer prodrugs **G1L-G3L** showed a decrease in diameter within the first 10 days before exhibiting constant average diameters, suggesting slow rearrangement over time of the polymer prodrugs within the nanoparticles.

Similarly, diglycolate-containing heterobifunctional polymer prodrugs, Gem-PI-digly-Dox (**G4dD** and **G5dD**) and Gem-PI-digly-Lap (**G1dL** and **G3dL**), were formulated into nanoparticles with average diameters in the 46–149 nm range (Table S2).

3.4. In vitro gemcitabine release

Amide bonds are stable in water but can be cleaved for instance by cathepsin [75], that are present in higher concentrations in lysosomes of tumor cells. The in vitro release of Gem from the different prodrug nanoparticles was monitored over time at 37 °C in pure human serum, to mimic the biological environment. Monofunctional Gem-PI (**G2**) nanoparticles showed a Gem release of 6.1 mol% after 24 h. Gem-PI-coPI-Dox (**G2coD1**) nanoparticles had a slightly higher Gem release than **G2** reaching 8.2 mol%. Conversely, heterobifunctional polymer prodrug nanoparticles Gem-PI-Dox (**G2D**) and Gem-PI-diglyDox (**G5dD**) had much slower Gem release kinetics than **G2**, leading to 1.6 and 1.9 mol% after 24 h (Fig. 7a). Importantly, nanoparticles containing Lap instead of Dox showed the same trends: Gem-PIcoPI-Lap (**G2coL1**) gave 8.3 mol% of released Gem, whereas heterobifunctional Gem-PI-Lap (**G2L**) and Gem-PI-digly-Lap (**G3dL**) nanoparticles both led to < 1 mol% of Gem released (Fig. 7b).

Moreover, all Gem release kinetics from monofunctional polymer prodrug nanoparticles rapidly reached a plateau within the first few hours. It suggested that, at least during the first 24 h, only surface-exposed Gem was able to be efficiently cleaved by enzymes [16] because the high colloidal stability of the nanoparticles prevented the drug buried in the nanoparticle core to be rapidly cleaved off the polymer. Such a significant difference in the Gem release pattern between heterobifunctional polymer prodrug nanoparticles and monofunctional counterparts (either prepared from Gem-PI alone or resulting from their *co*-nanoprecipitation with another monofunctional polymer prodrug) might be assigned to a change in the supramolecular organization of the polymer chains during the nanoparticle formation. Indeed, given the low M_n of the polymer and the different solubility of drugs (Gem is hydrophilic whereas Lap or Dox are hydrophobic), placement of Gem within, and at the surface of the nanoparticles, may be shifted toward the core of the nanoparticles when another drug is attached at the chain-end.

Surprisingly, we were not able to detect any release of Dox or Lap, regardless of the nature of the linker (i.e., succinate or diglycolate). This observation was at first glance unexpected since the diglycolate linker was supposed to promote the release of Lap (**G3dL**) and Dox (**G5dD**), as

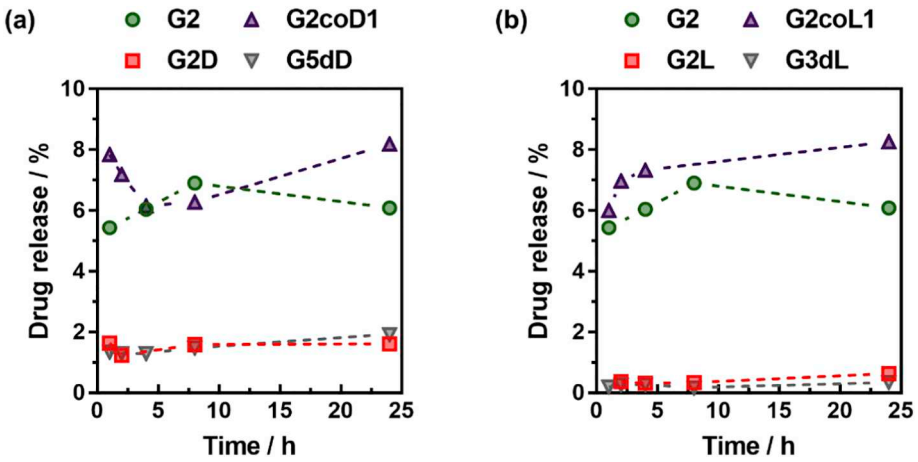

Fig. 7. Gem release profiles at 37 °C in human serum from (a) Gem-PI (**G2**), Gem-PIcoPI-Dox (**G2coD1**), Gem-PI-Dox (**G2D**) and Gem-PI-diglyDox (**G5dD**) and (b) Gem-PI (**G2**), Gem-PIcoPI-Lap (**G2coL1**), Gem-PI-Lap (**G2L**) and Gem-PI-digly-Lap (**G3dL**).

previously shown for other types of monofunctional polymer prodrug nanoparticles [16,17,20,21]. However, since Lap and Dox are both hydrophobic and likely localized into the core of the nanoparticles, their absence of release further confirmed the high colloidal stability of the nanoparticles (at least under the conditions and within the time frame of the drug release experiments), that prevented enzyme access and/or colloidal disassembly. Note also that in vitro experiments may not fully reflect the complexity of an in vivo tumor model, whose conditions (e.g., acidic pH in the tumor microenvironment, higher concentrations of specific enzymes, etc.) may contribute to induce a faster colloidal disassembly of the nanoparticles and thus a more significant drug release.

3.5. In vitro cell viability

The two series of heterobifunctional polymer prodrug nanoparticles, Gem-PI-Dox and Gem-PI-Lap, were tested for their cytotoxicity on human breast cancer cell line MCF-7, a model widely used to test these drugs and their combinations [41,52,53,57,58]. Given the high coupling efficiencies from ESR/UV measurements and the quantitative coupling efficiencies from ^{1}H NMR, equimolar drug ratios were considered for heterobifunctional polymer nanoparticles and nanoparticles combining both drugs. To determine the best way to transport and deliver a prodrug combination from nanocarriers, other formulation options were tested, such as the *co*-nanoprecipitation of monofunctional polymer prodrugs and the mixture of the two monofunctional polymer prodrug nanoparticles. Also, control formulations composed of monofunctional polymer prodrug nanoparticles from each drug were tested. The cells were incubated with increasing concentrations of the different prodrug nanoparticles or free drugs for 72 h to determine the IC_{50}.

First, bare (i.e., drug-free) PI nanoparticles were not cytotoxic on MCF-7 cells up to at least 2.5 μM; that is higher than the concentrations of the different prodrugs, thus excluding potential cytotoxicity of the vehicle (Fig. S10).

Regarding Gem/Dox combination (Fig. 8), free Dox led to an IC_{50} of 92 nM, whereas IC_{50} of free Gem and its 1:1 combination with Dox was as low as 7 and 6 nM, respectively (Table 4), showing the higher cytotoxicity of Gem compared to Dox on this cancer cell line. Also, no synergy was obtained for the combination of free drugs.

Second observation is that both monofunctional prodrug nanoparticles were less active than the corresponding free drugs (IC_{50} = 1.89 μM and 53 nM for **D1** and **G2**, respectively), which is somewhat expected since the drug needs to get cleaved off the polymer before regaining its activity. Also, free drugs are not (or poorly) subjected to early metabolization and degradation in vitro, hence exhibiting optimal cytotoxicity, conversely to in vivo where using

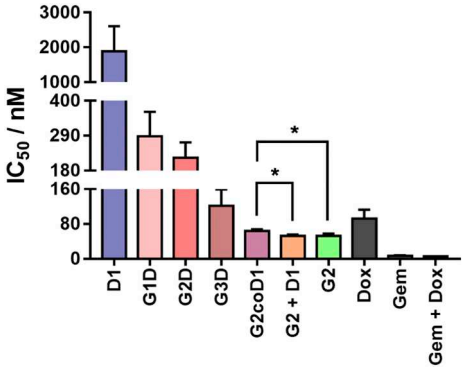

Fig. 8. IC_{50} values ± SD of Gem-PI-Dox (**G1D-G3D**), Gem-PI (**G2**), PI-Dox (**D1**), Gem-PIcoPI-Dox (**G2coD1**), Gem-PI + PI-Dox (**G2** + **D1**) nanoparticles, free Gem, free Dox and free Gem + Dox (1:1, mol:mol) determined by MTT test on MCF-7 cells after 72 h of incubation. (*$p < 0.05$, **G2** + **D1**, **G2** vs **G2coD1**).

Table 4
Half maximal inhibitory concentrations (IC_{50}) of free drugs (Gem, Dox, Lap, Gem + Lap, Gem + Dox), prodrug nanoparticles [Gem-PI (**G2**), Gem-PI-Dox (**G1D-G3D**), PI-Dox (**D1**), Gem-PIcoPI-Dox (**G2coD1**), Gem-PI-Lap (**G2L-G3L**), PI-Lap (**L1**) and Gem-PIcoPI-Lap (**G2coL1**)] and physical mixtures of nanoparticles (**G2** + **D1** and **G2** + **L1**).

Gem/Dox formulations	IC_{50} (nM)[a]	Gem/lap formulations	IC_{50} (nM)[a]
Gem	7 ± 2	**Gem**	7 ± 2
Dox	92 ± 21	**Lap**	6070 ± 1210
Gem + **Dox**	6 ± 1	**Gem** + **Lap**	5 ± 1
G2	53 ± 5	**G2**	54 ± 3
D1	1890 ± 720	**L1**	152 ± 40
G2 + **D1**	53 ± 3	**G2** + **L1**	44 ± 13
G2coD1	64 ± 4	**G2coL1**	33 ± 5
G1D	288 ± 77	**G2L**	214 ± 146
G2D	221 ± 48	**G3L**	282 ± 47
G3D	121 ± 38		

[a] Expressed as IC_{50} ± SD determined by MTT test after 72 h of incubation on MCF7 cells.

prodrugs takes on its full meaning (especially with Gem). Heterobifunctional Gem-PI-Dox nanoparticles gave decreasing IC_{50} values with the increase of the M_n, as IC_{50} = 288, 221 and 121 nM for **G1D**, **G2D** and **G3D**, respectively (Table 4). This IC_{50} vs M_n trend has already been observed for other types of "*drug-initiated*" polymer prodrug nanoparticles [17,21,29] and might be attributed to a better cell uptake for higher nanoparticle surface hydrophobicity when the Gem content is decreased. However, heterobifunctional Gem-PI-Dox

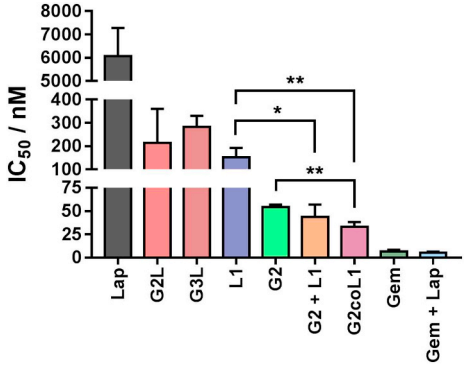

Fig. 9. IC_{50} values ± SD of Gem-PI-Lap (**G2L-G3L**), Gem-PI (**G2**), PI-Lap (**L1**), Gem-PIcoPI-Lap (**G2coL1**), Gem-PI + PI-Lap (**G2** + **L1**) nanoparticles, free Gem, free Lap and free Gem + Lap (1:1, mol:mol) determined by MTT test on MCF-7 cells after 72 h of incubation. (**$p < 0.01$ **G2coL1** vs **G2** or **L1**, *$p < 0.05$ **G2** + **L1** vs **L1**).

nanoparticles **G1D–G3D** were more cytotoxic than prodrug nanoparticles **D1**, but less than prodrug nanoparticles **G2** and monofunctional prodrugs either used as mixed formulations (**G2** + **D1**, IC_{50} = 53 nM) or resulting from a co-nanoprecipitation (**G2coD1**, IC_{50} = 64 nM). This result is in line with the drug release study reported in Fig. 7a, showing that release of Gem is much slower when Dox is attached at the other polymer chain-end. Replacing the succinate linker by a supposedly more labile diglycolate linker did not improve the cytotoxicity pattern (Fig. S11a), which is in agreement with the deep localization of Dox into the nanoparticle core and its poor accessibility to enzymes. It thus tends to support a different placement of each drug within the nanoparticles and its crucial role on the drug release and eventually its activity.

Interestingly, given that nanoparticles **D1** had a much higher IC_{50} than nanoparticles **G2**, the physical mixture of nanoparticles (**G2** + **D1**) had the same cytotoxicity than nanoparticles **G2**. However, co-nanoprecipitated prodrugs **G2coD1** led to slightly lower cytotoxicity than nanoparticles **G2** or **G2** + **D1**.

Evaluation of the Gem/Lap combination resulted in a quite different behavior (Fig. 9). Free Lap had a much higher IC_{50} (6.0 μM) than any other formulations. Interestingly, Lap-containing polymer prodrug nanoparticles drastically improved its anticancer activity, as PI-Lap (**L1**) had a much small IC_{50} value (152 nM). This enhancement can be assigned to improved solubility and therefore better cell uptake, as previously described for traditional Lap-loaded nanoparticulate systems [39–41]. Driven by its very high cytotoxicity, not only free Gem gave a very low IC_{50} (7 nM), but also its monofunctional prodrug (**G2**, IC_{50} = 54 nM), although to a lesser extent because of the prodrug nature as explained earlier. Due to the much higher free Gem activity compared to free Lap, the IC_{50} of their 1:1 combination was very similar to the one of free Gem (5 nM), but no synergy was noticed. However, heterotelechelic Gem-PI-Lap polymer prodrug nanoparticles led to higher IC_{50} values, similar to that of **L1**, ranging from 214 to 282 nM for **G2L** and **G3L**, respectively (Table 4). Again, switching from succinate to diglycolate linker between Lap and the polymer did not provide any benefit (Fig. S11b).

Remarkably, whereas the physical mixture **G2** + **L1** had a comparable IC_{50} (44 nM) than **G2**, similarly to what has been observed with Gem/Dox combination, the co-nanoprecipitated formulation (**G2coL1**) presented a lower IC_{50} than **G2** (33 nM), corresponding to a 39 and 78% decrease compared to IC_{50} values of **G2** and **L1**, respectively (Table 4). Using the combination index (CI), which is a well-established method to evaluate the combination effect [76], a synergistic effect was found for **G2coL1** (CI = 0.83), whereas the physical mixture **G2** + **L1** led to a simple additive effect (CI = 1.10). Therefore, co-administering Gem and Lap into the same nanoparticle led to synergistic effect in vitro. Nonetheless, the same effect was not present for heterotelechelic polymer, likely because of the drastically reduced Gem release kinetics (Fig. 7b) when Lap is attached at the other chain-end.

These findings showed that, in the context of combination therapy, the nature/properties of each drug and the way they are transported and organized into a nanocarrier, are of paramount importance for the overall therapeutic efficacy. Indeed, whereas heterobifunctional polymer prodrug nanoparticles based on Agm/Dox combination gave synergistic effect [29], monofunctional polymer prodrug formulations based on the Gem/Dox combination (**G2** and **G2coD1** and **G2** + **D1**) were the most cytotoxic, and only co-nanoprecipitated monofunctional Gem/Dox prodrugs **G2coL1** led to synergistic effect. It therefore suggested that each combination of drugs may act differently and finding optimal conditions is a case-by-case study, that can be easily and efficiently investigated through our synthetic approach.

4. Conclusion

In this work, we synthesized two different and well-defined heterotelechelic polymer prodrug nanoparticles for combination therapy. The methodology was based on the "*drug-initiated*" method, during which a small polymer chain was grown in a controlled fashion from the first drug by NMP, before end-capping the polymer chain-end by a nitroxide bearing the second drug of interest under nitroxide exchange reaction. We successfully applied this approach to Gem/Dox and Gem/Lap, which are combinations of high clinical relevance, and proved that it is a robust, versatile yet simple construction methodology for drug delivery purposes.

To highlight the importance of the way drug combinations are transported, heterotelechelic polymer prodrug nanoparticles were evaluated in terms of drug release and cytotoxicity together with monofunctional polymer prodrug formulations, either independent, physically mixed or formulated by co-nanoprecipitation. The results revealed that the nature and properties of the selected drugs had a tremendous effect on the outcome of the cytotoxicity, likely deriving from different spatial organization of the different drugs within the nanoparticles. Indeed, whereas Gem/Dox combination did not show any improvement over monofunctional therapies, co-nanoprecipitation of Gem/Lap prodrugs led to synergistic effect, which represents the first nanocarrier for the delivery of Gem and Lap together.

Although the purpose of this study was not to find the best optimal ratios between the two drugs from each combination, but rather to show a certain degree of universality of the synthetic methodology and to compare different formulation strategies, such further studies could be performed by readily tuning the amounts of drugs by playing with the nitroxide exchange reaction yield.

Acknowledgement

This work was supported by the European Union's Horizon 2020 research and innovation programme under Marie Skłodowska Curie grant agreement no. 642028 (NABBA). The authors thank the Service de Microscopie Electronique (UFR de Biologie Intégrative, Université Paris-Sud) for Cryo-TEM analyses and Stéphanie Nicolaÿ for mass spectrometry analyses (Service d'Analyses des Médicaments et Métabolites (Institut Paris-Sud d'Innovation Therapeutique (IPSIT), Université Paris-Sud). Arkema is warmly acknowledged for kindly providing the SG1 nitroxide. CNRS and Université Paris-Sud are also acknowledged for financial support.

Appendix A. Supplementary data

Supplementary data to this article can be found online at https://doi.org/10.1016/j.jconrel.2018.12.047.

References

[1] R.T. Eastman, D.A. Fidock, Artemisinin-based combination therapies: a vital tool in efforts to eliminate malaria, Nat. Rev. Microbiol. 7 (2009) 864.
[2] F. Nosten, P. Brasseur, Combination therapy for malaria, Drugs 62 (2002) 1315–1329.
[3] A.S. Perelson, P. Essunger, Y. Cao, M. Vesanen, A. Hurley, K. Saksela, M. Markowitz, D.D. Ho, Decay characteristics of HIV-1-infected compartments during combination therapy, Nature 387 (1997) 188.
[4] M. Egger, B. Hirschel, P. Francioli, P. Sudre, M. Wirz, M. Flepp, M. Rickenbach, R. Malinverni, P. Vernazza, M. Battegay, Impact of new antiretroviral combination therapies in HIV infected patients in Switzerland: prospective multicentre study, BMJ 315 (1997) 1194–1199.
[5] B. Al-Lazikani, U. Banerji, P. Workman, Combinatorial drug therapy for cancer in the post-genomic era, Nat. Biotechnol. 30 (2012) 679.
[6] C.-M.J. Hu, L. Zhang, Nanoparticle-based combination therapy toward overcoming drug resistance in cancer, Biochem. Pharmacol. 83 (2012) 1104–1111.
[7] F. Greco, M.J. Vicent, Combination therapy: opportunities and challenges for polymer–drug conjugates as anticancer nanomedicines, Adv. Drug Deliv. Rev. 61 (2009) 1203–1213.
[8] P. Parhi, C. Mohanty, S.K. Sahoo, Nanotechnology-based combinational drug delivery: an emerging approach for cancer therapy, Drug Discov. Today 17 (2012) 1044–1052.
[9] X. Xu, W. Ho, X. Zhang, N. Bertrand, O. Farokhzad, Cancer nanomedicine: from targeted delivery to combination therapy, Trends Mol. Med. 21 (2015) 223–232.
[10] V. Delplace, P. Couvreur, J. Nicolas, Recent trends in the design of anticancer polymer prodrug nanocarriers, Polym. Chem. 5 (2014) 1529–1544.
[11] F. Kratz, I.A. Müller, C. Ryppa, A. Warnecke, Prodrug strategies in anticancer chemotherapy, Chem. Med. Chem. 3 (2008) 20–53.
[12] J. Nicolas, Drug-initiated synthesis of polymer prodrugs: combining simplicity and efficacy in drug delivery, Chem. Mater. 28 (2016) 1591–1606.
[13] S. Harrisson, J. Nicolas, A. Maksimenko, D.T. Bui, J. Mougin, P. Couvreur, Nanoparticles with in vivo anticancer activity from polymer prodrug amphiphiles prepared by living radical polymerization, Angew. Chem. Int. Ed. 52 (2013) 1678–1682.
[14] D. Trung Bui, A. Maksimenko, D. Desmaële, S. Harrisson, C. Vauthier, P. Couvreur, J. Nicolas, Polymer prodrug nanoparticles based on naturally occurring isoprenoid for anticancer therapy, Biomacromolecules 14 (2013) 2837–2847.
[15] A. Maksimenko, D.T. Bui, D. Desmaële, P. Couvreur, J. Nicolas, Significant tumor growth inhibition from naturally occurring lipid-containing polymer prodrug nanoparticles obtained by the drug-initiated method, Chem. Mater. 26 (2014) 3606–3609.
[16] E. Guégain, J. Tran, Q. Deguettes, J. Nicolas, Degradable polymer prodrugs with adjustable activity from drug-initiated radical ring-opening copolymerization, Chem. Sci. (2018), https://doi.org/10.1039/C1038SC02256A.
[17] Y. Bao, E. Guegain, J. Mougin, J. Nicolas, Self-stabilized, hydrophobic or PEGylated paclitaxel polymer prodrug nanoparticles for cancer therapy, Polym. Chem. 9 (2018) 687–698.
[18] B. Louage, M.J. Van Steenbergen, L. Nuhn, M.D. Risseeuw, I. Karalic, J. Winne, S. Van Calenbergh, W.E. Hennink, B.G. De Geest, Micellar paclitaxel-initiated raft polymer conjugates with acid-sensitive behavior, ACS Macro Lett. 6 (2017) 272–276.
[19] B. Louage, L. Nuhn, M.D. Risseeuw, N. Vanparijs, R. De Coen, I. Karalic, S. Van Calenbergh, B.G. De Geest, Well-defined polymer–paclitaxel prodrugs by a grafting-from-drug approach, Angew. Chem. Int. Ed. 55 (2016) 11791–11796.
[20] Y. Bao, T. Boissenot, E. Guégain, D. Desmaële, S. Mura, P. Couvreur, J. Nicolas, Simple synthesis of cladribine-based anticancer polymer prodrug nanoparticles with tunable drug delivery properties, Chem. Mater. 28 (2016) 6266–6275.
[21] Y. Bao, J. Nicolas, Structure–cytotoxicity relationship of drug-initiated polymer prodrug nanoparticles, Polym. Chem. 8 (2017) 5174–5184.
[22] G. Moad, E. Rizzardo, S.H. Thang, Living radical polymerization by the raft process–a second update, Aust. J. Chem. 62 (2009) 1402–1472.
[23] J. Nicolas, Y. Guillaneuf, C. Lefay, D. Bertin, D. Gigmes, B. Charleux, Nitroxide-mediated polymerization, Prog. Polym. Sci. 38 (2013) 63–235.
[24] H.-C. Yang, J. Silverman, J.J. Wozniak, Low Temperature Heat Shrinkable Polymer Material, (1986) (US 4596728).
[25] C. Cheng, K. Qi, E. Khoshdel, K.L. Wooley, Tandem synthesis of core − shell brush copolymers and their transformation to peripherally cross-linked and hollowed nanostructures, J. Am. Chem. Soc. 128 (2006) 6808–6809.
[26] S.Y. Chen, Y. Huang, R.C.C. Tsiang, Ozonolysis efficiency of PS-b-PI block copolymers for forming nanoporous polystyrene, J. Polym. Sci. A Polym. Chem. 46 (2008) 1964–1973.
[27] S. Sato, Y. Honda, M. Kuwahara, T. Watanabe, Degradation of vulcanized and nonvulcanized polyisoprene rubbers by lipid peroxidation catalyzed by oxidative enzymes and transition metals, Biomacromolecules 4 (2003) 321–329.
[28] K. Rose, A. Steinbüchel, Biodegradation of natural rubber and related compounds: recent insights into a hardly understood catabolic capability of microorganisms, Appl. Environ. Microbiol. 71 (2005) 2803–2812.
[29] D. Vinciguerra, S. Denis, J. Mougin, M. Jacobs, Y. Guillaneuf, S. Mura, P. Couvreur, J. Nicolas, A facile route to heterotelechelic polymer prodrug nanoparticles for imaging, drug delivery and combination therapy, J. Control. Release 286 (2018) 425–438.
[30] Y. Guillaneuf, P.-E. Dufils, L. Autissier, M. Rollet, D. Gigmes, D. Bertin, Radical chain end chemical transformation of SG1-based polystyrenes, Macromolecules 43 (2009) 91–100.
[31] M.J. Vicent, F. Greco, R.I. Nicholson, A. Paul, P.C. Griffiths, R. Duncan, Polymer therapeutics designed for a combination therapy of hormone-dependent cancer, Angew. Chem. Int. Ed. 44 (2005) 4061–4066.
[32] F. Greco, M.J. Vicent, S. Gee, A.T. Jones, J. Gee, R.I. Nicholson, R. Duncan, Investigating the mechanism of enhanced cytotoxicity of HPMA copolymer–Dox–AGM in breast cancer cells, J. Control. Release 117 (2007) 28–39.
[33] D. Vinciguerra, J. Tran, J. Nicolas, Telechelic polymers from reversible-deactivation radical polymerization for biomedical applications, Chem. Commun. 54 (2018) 228–240.
[34] L.W. Hertel, G.B. Boder, J.S. Kroin, S.M. Rinzel, G.A. Poore, G.C. Todd, G.B. Grindey, Evaluation of the antitumor activity of gemcitabine (2′, 2′-difluoro-2′-deoxycytidine), Cancer Res. 50 (1990) 4417–4422.
[35] V. Heinemann, Y.-Z. Xu, S. Chubb, A. Sen, L.W. Hertel, G.B. Grindey, W. Plunkett, Cellular elimination of 2′, 2′-difluorodeoxycytidine 5′-triphosphate: a mechanism of self-potentiation, Cancer Res. 52 (1992) 533–539.
[36] C. Galmarini, J. Mackey, C. Dumontet, Nucleoside analogues: mechanisms of drug resistance and reversal strategies, Leukemia 15 (2001) 875.
[37] R.H. Blum, S.K. Carter, Adriamycin: a new anticancer drug with significant clinical activity, Ann. Intern. Med. 80 (1974) 249–259.
[38] W. Xia, R.J. Mullin, B.R. Keith, L.-H. Liu, H. Ma, D.W. Rusnak, G. Owens, K.J. Alligood, N.L. Spector, Anti-tumor activity of GW572016: a dual tyrosine kinase inhibitor blocks EGF activation of EGFR/erbB2 and downstream Erk1/2 and AKT pathways, Oncogene 21 (2002) 6255.
[39] H. Gao, S. Cao, C. Chen, S. Cao, Z. Yang, Z. Pang, Z. Xi, S. Pan, Q. Zhang, X. Jiang, Incorporation of lapatinib into lipoprotein-like nanoparticles with enhanced water solubility and anti-tumor effect in breast cancer, Nanomedicine 8 (2013) 1429–1442.
[40] X. Wan, X. Zheng, X. Pang, Z. Zhang, T. Jing, W. Xu, Q. Zhang, The potential use of lapatinib-loaded human serum albumin nanoparticles in the treatment of triple-negative breast cancer, Int. J. Pharm. 484 (2015) 16–28.
[41] Z.J. Huo, S.J. Wang, Z.Q. Wang, W.S. Zuo, P. Liu, B. Pang, K. Liu, Novel nanosystem to enhance the antitumor activity of lapatinib in breast cancer treatment: therapeutic efficacy evaluation, Cancer Sci. 106 (2015) 1429–1437.
[42] E. Rivera, V. Valero, B. Arun, M. Royce, R. Adinin, K. Hoelzer, R. Walters, J.L. Wade III, L. Pusztai, G.N. Hortobagyi, Phase II study of pegylated liposomal doxorubicin in combination with gemcitabine in patients with metastatic breast cancer, J. Clin. Oncol. 21 (2003) 3249–3254.
[43] A. Fabi, G. Ferretti, P. Papaldo, N. Salesi, M. Ciccarese, V. Lorusso, P. Carlini, A. Carpino, M. Mottolese, A.M. Cianciulli, Pegylated liposomal doxorubicin in combination with gemcitabine: a phase II study in anthracycline-naive and anthracycline pretreated metastatic breast cancer patients, Cancer Chemother. Pharmacol. 57 (2006) 615–623.
[44] G. Perez-Manga, A. Lluch, E. Alba, J. Moreno-Nogueira, M. Palomero, J. Garcia-Conde, D. Khayat, N. Rivelles, Gemcitabine in combination with doxorubicin in advanced breast cancer: final results of a phase II pharmacokinetic trial, J. Clin. Oncol. 18 (2000) 2545–2552.
[45] T. Yang, C. Wang, R. Hsieh, J. Chen, M. Fung, Gemcitabine and doxorubicin for the treatment of patients with advanced hepatocellular carcinoma: a phase I–II trial, Ann. Oncol. 13 (2002) 1771–1778.
[46] G. Lombardi, F. Zustovich, F. Farinati, U. Cillo, A. Vitale, G. Zanus, M. Donach, M. Farina, S. Zovato, D. Pastorelli, Pegylated liposomal doxorubicin and gemcitabine in patients with advanced hepatocellular carcinoma, Cancer 117 (2011) 125–133.
[47] E. Rivera, V. Valero, L. Syrewicz, Z. Rahman, F.L. Esteva, R.L. Theriault, M.M. Rosales, D. Booser, J.L. Murray, R.C. Bast Jr., Phase I study of stealth liposomal doxorubicin in combination with gemcitabine in the treatment of patients with metastatic breast cancer, J. Clin. Oncol. 19 (2001) 1716–1722.
[48] G. D'agostino, G. Ferrandina, M. Ludovisi, A. Testa, D. Lorusso, N. Gbaguidi, E. Breda, S. Mancuso, G. Scambia, Phase II study of liposomal doxorubicin and gemcitabine in the salvage treatment of ovarian cancer, Br. J. Cancer 89 (2003) 1180.
[49] J.-P. Jacquin, C. Chargari, J. Thorin, D. Mille, A. Mélis, H. Orfeuvre, G. Clavreul, L. Chaigneau, A. Nourissat, C. Dumanoir, Phase II trial of pegylated liposomal doxorubicin in combination with gemcitabine in metastatic breast cancer patients, Am. J. Clin. Oncol. 35 (2012) 18–21.
[50] N.B. Haas, X. Lin, J. Manola, M. Pins, G. Liu, D. McDermott, D. Nanus, E. Heath, G. Wilding, J. Dutcher, A phase II trial of doxorubicin and gemcitabine in renal cell carcinoma with sarcomatoid features: ECOG 8802, Med. Oncol. 29 (2012) 761–767.
[51] T. Lammers, V. Subr, K. Ulbrich, P. Peschke, P.E. Huber, W.E. Hennink, G. Storm, Simultaneous delivery of doxorubicin and gemcitabine to tumors in vivo using prototypic polymeric drug carriers, Biomaterials 30 (2009) 3466–3475.
[52] D. Liu, Y. Chen, X. Feng, M. Deng, G. Xie, J. Wang, L. Zhang, Q. Liu, P. Yuan, Micellar nanoparticles loaded with gemcitabine and doxorubicin showed synergistic effect, Colloids Surf. B: Biointerfaces 113 (2014) 158–168.
[53] R. Nahire, M.K. Haldar, S. Paul, A.H. Ambre, V. Meghnani, B. Layek, K.S. Katti, K.N. Gange, J. Singh, K. Sarkar, Multifunctional polymersomes for cytosolic delivery of gemcitabine and doxorubicin to cancer cells, Biomaterials 35 (2014) 6482–6497.
[54] C.E. Geyer, J. Forster, D. Lindquist, S. Chan, C.G. Romieu, T. Pienkowski, A. Jagiello-Gruszfeld, J. Crown, A. Chan, B. Kaufman, Lapatinib plus capecitabine for HER2-positive advanced breast cancer, N. Engl. J. Med. 355 (2006) 2733–2743.
[55] D. Cameron, M. Casey, M. Press, D. Lindquist, T. Pienkowski, C.G. Romieu, S. Chan, A. Jagiello-Gruszfeld, B. Kaufman, J. Crown, A phase III randomized comparison of lapatinib plus capecitabine versus capecitabine alone in women with advanced breast cancer that has progressed on trastuzumab: updated efficacy and biomarker analyses, Breast Cancer Res. Treat. 112 (2008) 533–543.

[56] Q. Ryan, A. Ibrahim, M.H. Cohen, J. Johnson, C.-w. Ko, R. Sridhara, R. Justice, R. Pazdur, FDA drug approval summary: lapatinib in combination with capecitabine for previously treated metastatic breast cancer that overexpresses HER-2, Oncologist 13 (2008) 1114–1119.
[57] C.-l. Dai, A.K. Tiwari, C.-P. Wu, X.-d. Su, S.-R. Wang, D.-g. Liu, C.R. Ashby, Y. Huang, R.W. Robey, Y.-j. Liang, Lapatinib (Tykerb, GW572016) reverses multidrug resistance in cancer cells by inhibiting the activity of ATP-binding cassette subfamily B member 1 and G member 2, Cancer Res. 68 (2008) 7905–7914.
[58] S.-Y. Chun, Y.-S. Kwon, K.-S. Nam, S. Kim, Lapatinib enhances the cytotoxic effects of doxorubicin in MCF-7 tumorspheres by inhibiting the drug efflux function of ABC transporters, Biomed. Pharmacother. 72 (2015) 37–43.
[59] I. Park, K. Lee, H. Kang, S. Kim, S. Lee, S. Jung, Y. Kwon, K. Shin, K. Ko, B. Nam, J. Ro, A phase Ib study of preoperative lapatinib, paclitaxel, and gemcitabine combination therapy in women with HER2-positive early breast cancer, Investig. New Drugs 30 (2011) 1972–1977.
[60] G. Daugaard, L. Sengeløv, M. Agerbaek, C.N. Sternberg, C. Van Herpen, S. Collette, S. Marreaud, E.O.f. Research, T.o. Cancer, Phase I results from a study of lapatinib with gemcitabine and cisplatin (GC) in advanced/metastatic bladder cancer, J. Clin. Oncol. 31 (2013) (252–252).
[61] L. Cerbone, C.N. Sternberg, L. Sengeløv, M. Agerbaek, C. Van Herpen, S. Marreaud, S. Collette, J. Zhang, G. Daugaard, Results from a phase I study of lapatinib with gemcitabine and cisplatin in advanced or metastatic bladder cancer: EORTC Trial 30061, Oncology 90 (2016) 21–28.
[62] R. Van Der Noll, W. Smit, A. Wymenga, D. Boss, M. Grob, A. Huitema, H. Rosing, M. Tibben, M. Keessen, H. Rehorst, Phase I and pharmacological trial of lapatinib in combination with gemcitabine in patients with advanced breast cancer, Investig. New Drugs 33 (2015) 1197–1205.
[63] H.L. Gómez, S. Neciosup, C. Tosello, M. Mano, J. Bines, G. Ismael, P.X. Santi, H. Pinczowski, Y. Nerón, M. Fanelli, A phase II randomized study of lapatinib combined with capecitabine, vinorelbine, or gemcitabine in patients with HER2-positive metastatic breast cancer with progression after a taxane (Latin American Cooperative Oncology Group 0801 Study), Clin. Breast Cancer 16 (2016) 38–44.
[64] J.G. Blesa, J.L. Canales, V.A. Candel, One year of complete clinical response in a metastatic breast cancer patient treated with a combination of lapatinib and gemcitabine, Curr. Oncol. 17 (2010) 64.
[65] H. Safran, T. Miner, N. Bahary, S. Whiting, C.D. Lopez, W. Sun, K. Charpentier, J. Shipley, E. Anderson, B. McNulty, Lapatinib and gemcitabine for metastatic pancreatic cancer: a phase II study, Am. J. Clin. Oncol. 34 (2011) 50–52.
[66] V. Narayan, R. Mamtani, S. Keefe, T. Guzzo, S.B. Malkowicz, D.J. Vaughn, Cisplatin, gemcitabine, and lapatinib as neoadjuvant therapy for muscle-invasive bladder cancer, Cancer Res. Treat. 48 (2016) 1084–1091.
[67] S. Sengupta, D. Eavarone, I. Capila, G. Zhao, N. Watson, T. Kiziltepe, R. Sasisekharan, Temporal targeting of tumour cells and neovasculature with a nanoscale delivery system, Nature 436 (2005) 568.
[68] Y. Bae, T.A. Diezi, A. Zhao, G.S. Kwon, Mixed polymeric micelles for combination cancer chemotherapy through the concurrent delivery of multiple chemotherapeutic agents, J. Control. Release 122 (2007) 324–330.
[69] S. Harrisson, P. Couvreur, J. Nicolas, Simple and efficient copper metal-mediated synthesis of alkoxyamine initiators, Polym. Chem. 2 (2011) 1859–1865.
[70] D. Benoit, V. Chaplinski, R. Braslau, C.J. Hawker, Development of a universal alkoxyamine for living free radical polymerizations, J. Am. Chem. Soc. 121 (1999) 3904–3920.
[71] D. Benoit, E. Harth, P. Fox, R.M. Waymouth, C.J. Hawker, Accurate structural control and block formation in the living polymerization of 1,3-dienes by nitroxide-mediated procedures, Macromolecules 33 (2000) 363–370.
[72] H. Fessi, F. Puisieux, J.P. Devissaguet, N. Ammoury, S. Benita, Nanocapsule formation by interfacial polymer deposition following solvent displacement, Int. J. Pharm. 55 (1989) R1–R4.
[73] A. Maksimenko, J. Mougin, S. Mura, E. Sliwinski, E. Lepeltier, C. Bourgaux, S. Lepêtre, F. Zouhiri, D. Desmaële, P. Couvreur, Polyisoprenoyl gemcitabine conjugates self assemble as nanoparticles, useful for cancer therapy, Cancer Lett. 334 (2013) 346–353.
[74] S.M. Ansell, S.A. Johnstone, P.G. Tardi, L. Lo, S. Xie, Y. Shu, T.O. Harasym, N.L. Harasym, L. Williams, D. Bermudes, Modulating the therapeutic activity of nanoparticle delivered paclitaxel by manipulating the hydrophobicity of prodrug conjugates, J. Med. Chem. 51 (2008) 3288–3296.
[75] P. Couvreur, B. Stella, L.H. Reddy, H. Hillaireau, C. Dubernet, D. Desmaële, S. Lepêtre-Mouelhi, F. Rocco, N. Dereuddre-Bosquet, P. Clayette, Squalenoyl nanomedicines as potential therapeutics, Nano Lett. 6 (2006) 2544–2548.
[76] J. Foucquier, M. Guedj, Analysis of drug combinations: current methodological landscape, Pharmacol. Res. Perspect. 3 (2015) e00149.